Peer-reviewed version available at Genes 2020, 11, 126; doi:10.3390/genes11020126

Article

Pulmonary Hypertension Remodels the Genomic Fabrics of Major Functional Pathways

Rajamma Mathew [1,2], Jing Huang [1], Sanda Iacobas [3] and Dumitru A Iacobas [4,*]

[1] Department of Pediatrics, New York Medical College, Valhalla, NY 10595, U.S.A.
[2] Department of Physiology, New York Medical College, Valhalla, NY 10595, U.S.A.
[3] Department of Pathology, New York Medical College, Valhalla, NY 10595, U.S.A.
[4] Personalized Genomics Laboratory, Center for Computational Systems Biology, Roy G Perry College of Engineering, Prairie View A&M University, Prairie View, TX77446, U.S.A.
* Correspondence: daiacobas@pvamu.edu; Tel.: +1(936)261-9926

Abstract: Pulmonary hypertension (PH) is a serious disorder with high morbidity and mortality rate. We analyzed the right ventricular systolic pressure (RVSP), right ventricular hypertrophy (RVH), lung histology and transcriptomes of six weeks old male rats with PH induced by: 1) hypoxia (HO), 2) administration of monocrotaline (CM) or 3) administration of monocrotaline and exposure to hypoxia (HM). The results in PH rats were compared to those in control rats (CO). After four weeks exposure, increased RVSP and RVH, pulmonary arterial wall thickening, and alteration of the lung transcriptome were observed in all PH groups. The HM group exhibited the largest alterations and also neointimal lesions and obliteration of lumen in small arteries. We found that the PH increased the expression of caveolin1, matrix metallopeptidase 2 and numerous inflammatory and cell proliferation genes. The cell-cycle, vascular smooth muscle contraction and the oxidative phosphorylation pathways, as well as their interplay were largely perturbed. Our results also suggest that the up-regulated *Rhoa* (ras homolog family member A) mediates its action through expression coordination with several ATPases. The upregulation of antioxidant genes and the extensive mitochondrial damage observed especially in HM group, indicate metabolic shift towards aerobic glycolysis.

Keywords: aerobic glycolysis; caveolin1; hypoxia; monocrotaline; oxidative phosphorylation; RhoA

1. Introduction

Pulmonary hypertension (PH), characterized by increasing pulmonary artery pressure and vascular resistance [1] is a serious complication of a number of unrelated cardiopulmonary, inflammatory and autoimmune diseases as well as of drug toxicity. PH is characterized by the endothelial dysfunction, enhanced vasoconstrictor reactivity, activation of proliferative and anti-apoptotic pathways, vascular remodeling, elevated pulmonary artery pressure and right ventricular hypertrophy (RVH), leading to right ventricular failure and premature death.

Recently updated PH classification maintains the original five groups with some modification [2]. The term Pulmonary Arterial Hypertension (PAH) is assigned to Group1. It includes idiopathic (IPAH) and heritable PAH (HPAH), PAH associated with congenital heart diseases, drug toxicity, connective tissue disorders, portal hypertension, HIV infection and schistosomiasis. The average survival time in patients with PAH without treatment was reported in 1991 to be around 2.8 years [3]. Despite the improvement in quality of life, the current therapy fails to reverse or halt the progression of the vascular disease [4]. Progressive pulmonary vascular changes lead to neointimal lesions resulting in the irreversibility of the PH [5]. The five-year survival rate remains poor in patients with IPAH, HPAH and PAH associated with anorexigenic drug treatment [6, 7]. PAH diagnosis is often delayed because of the vague symptoms. By the time the diagnosis is made, most of the patients have significant pathological changes in the pulmonary vasculature, which poses a serious challenge to therapeutic measures.

Mutations of genes *BMPR2* (bone morphogenetic protein receptor type 2), *ACVRL1* (activin A receptor like type 1), *ENG* (endoglin), *SMAD9* (SMAD family member 9), *CAV1* (caveolin 1) and *KCNK3* (potassium two pore domain channel subfamily K member 3) are well documented causes of PAH. About 20% of people with *BMPR2* mutation develop PH, indicating that a second hit is necessary. Furthermore, loss of Bmpr2 has been observed in the monocrotaline (MCT) and hypoxia models of PH [8]. *BMPR2* gene therapy fails to inhibit MCT-induced PH; however, administration of GDF2 (growth differentiation factor 2, also known as BMP9) was shown to have preventive and reversal effect on experimental PH [9, 10]. *BMPR2* is predominantly expressed in endothelial cells and a part of it co-localizes with CAV1 [11], and the loss of BMPR2 increases the susceptibility to DNA damage [12]. The increased expression of *SMURF1* (SMAD specific E3 ubiquitin protein ligase 1) that induces lysosomal and proteosomal degradation of BMPR2 has been shown to occur in patients with PAH, as well as in hypoxia and MCT-induced PH. Furthermore, Smurf1 deletion protects mice from PAH [8, 13]. Robust expression of *Nos3* (nitric oxide synthase 3) has been reported in plexiform lesions in PAH [14].

The importance of CAV1 in PH is supported by recent observations that patients with *CAV1* mutation develop PAH [15]. In addition, *Cav1* knockout mice develop PH which can be reversed by reconstituting endothelial Cav1 [16, 17]. Extensive loss of endothelial CAV1 accompanied by enhanced expression of *CAV1* in vascular smooth muscle cells (VSMC) has been reported in IPAH, HPAH, in PAH associated with congenital heart defect and drug toxicity [11, 18-20] and in infants with bronchopulmonary dysplasia and evidence of inflammation [19]. Furthermore, pulmonary artery smooth muscle cells isolated from patients with PH revealed enhanced expression of *CAV1*, increased capacitative Ca^{2+} entry and increased DNA synthesis which could be blocked by *CAV1*siRNA [18]. Inflammation has been shown to play a significant role in PH and CAV1 modulates inflammatory response. Furthermore, *Cav1* knockout mice have increased levels of circulating pro-inflammatory cytokines [21]. In the experimental models of PH, loss of Cav1 has been shown to be associated with increased levels and bioactivity of Il6, and activation of *Stat3* and *Nfkb1*. Rescue of Cav1 results in the attenuation of PH [22, 23].

We have previously shown that exposing the MCT-injected rats to hypoxia accelerates the PH disease process. By 4 weeks, there is extensive endothelial Cav1 loss, accompanied by enhanced expression of Cav1 in VSMC of a large number of arteries, resulting in near normalization of total Cav1 protein expression in the lungs. Several of the arteries with enhanced expression of Cav1 displayed neointima formation. Moreover, lung *Nos3* expression in this group was near normal levels unlike the group MCT injected rats exposed to normal atmosphere, where the lung Nos3 level was low. Importantly, lung sections from IPAH and HPAH patients revealed similar sequence of events: 1) loss of endothelial CAV1 and endothelial cell disruption, 2) enhanced expression of CAV1 in VSMC and 3) presence of neointima only in arteries that displayed enhanced expression of CAV-1 in VSMC [20]. In vitro studies with pulmonary artery endothelial cells from IPAH patients have CAV1 degradation owing to sustained NOS3 and SRC signaling [24]. Furthermore, loss of CAV1 in EC has been shown to cause mitochondrial stress, increase oxidative stress and metabolic switch [25].

In this article, we present our observations on the 4-weeks weight gain, right ventricular systolic pressure (RVSP), right ventricle hypertrophy (RVH), pulmonary vascular histology and lung transcriptomes of three rat models of PH with respect to the control group.

2. Materials and Methods

Animals: 6 weeks old male Sprague-Dawley rats (150-175g) were obtained from Charles River Wilmington, MA. Rats were allowed to acclimatize in the animal facility for 5 days, and had free access to laboratory chow and water. The rats were kept in the Animal facility maintained at 22°C and 12 hours each of light and dark cycle. The experiments respected the guiding principles for the use and care of laboratory animals of the American Physiological Society and the National Institutes of Health. The Institutional Animal Care and Use Committee at New York Medical College approved the protocol "Mechanism of neointima formation in pulmonary hypertension" (approval # 4-1-0113/2014, P.I. R.M). Rats were divided into 4 groups (n = 8/gr.). Gr1 - Control rats (**CO),** maintained

Peer-reviewed version available at Genes 2020, 11, 126; doi:10.3390/genes11020126

in room air. Gr2 (**CM**) rats received a single subcutaneous injection of monocrotaline (MCT 40 mg/kg) and kept in room air. Gr3 (**HO**) rats subjected to hypobaric hypoxia (atmospheric pressure 380 mmHg). Gr4 (**HM**), rats received MCT 40 mg/kg and were subjected to hypobaric hypoxia starting on day1. The hypoxia chamber was opened twice per week for 15 min to weigh the rats, replenish food and water, and to provide clean bedding similar to the other rats in room air. At the end of 4 weeks, these rats were studied.

Chemicals and antibodies: All chemicals were purchased from Sigma Aldrich, St Louis, MO.

Measurement of Right Ventricular Systolic Pressure (RVSP): As previously described [26], rats were anesthetized with an intraperitoneal injection of xylazine (6 mg/kg) and ketamine (60mg/kg). Through an incision in the neck, the trachea was exposed and cannulated with PE 240 tubing, and the rat ventilated in room air (≈70-80 breaths/min). The chest was opened, PE 50 tubing with a small needle inserted into the right ventricle, and the pressure recorded on a Grass polygraph (model 7E). At the end of the pressure measurements, the lungs were perfused with autoclaved normal saline to remove blood. The left lung and the heart were placed in 10% buffered formaldehyde. The right lung was quickly frozen in liquid nitrogen and stored at -80oC for transcriptomic analysis at a later date.

Assessment of Right Ventricular Hypertrophy (RVH): A week later, the heart was removed from formaldehyde and atria trimmed. The free wall of the right ventricle (RV) was separated from the left ventricle (LV) and the septum (S) and weighted. The RVH was calculated for all groups as:

$$RVH^{(PH)} \equiv \overline{\left(\frac{RV}{LV+S}\right)_{weight}^{(PH)}} \Big/ \overline{\left(\frac{RV}{LV+S}\right)_{weight}^{(CO)}} \quad , \quad \forall (PH) = (HO),(CM),(HM) \tag{1}$$

The right ventricular hypertrophy occurs when the average RV/(LV+S)(PH)) is significantly ($p < 0.05$) larger than RV/(LV+S)(CO) (i.e. RVH significantly larger than 1).

Histology: Formalin preserved lung tissue was processed for paraffin block. Five to 6 μm sections were cut and stained with hematoxylin and eosin (H&E) for evaluation of the pulmonary vasculature.

Microarray: Lungs were quickly removed, frozen in liquid nitrogen and stored at -80o C. Total RNA was extracted with Qiagen RNeasy minikit (www.Qiagen.com), concentration determined with a NanoDrop ND-2000 Spectrophotometer (http://www.nanodrop.com) and purity with Agilent RNA 6000 Nano kit in an Agilent 2100 Bioanalyzer (www.agilent.com). Total RNA was then reverse transcribed in the presence of Cy3/Cy5 dUTP and the incorporation of the fluorescent tags determined again with the nanodrop. Differently labeled samples of biological replicates were hybridized over night with Agilent 60 mer 4x44k whole genome rat V2 arrays (#G2519F). Our optimized protocol [27] and the "multiple yellow" strategy [28] were used to profile each "condition" in four biological replicas. The arrays were scanned with an Agilent G2539A dual laser scanner and primary analysis performed with (Agilent) Feature Extraction 11.1 software. All spots affected by local corruption or with foreground fluorescence less than twice the background were disregarded and data normalized and filtered following our standard procedure [29].

Transcriptomic analysis: A gene was considered as significantly regulated if the absolute fold-change exceeded the cut-off calculated for that gene [30]. The cut-off (CUT, Eq. 1) accounts for the observed expression variability of that gene in the compared conditions and the existence of several spots probing it redundantly in the microarray. The non-uniform expression variability among the genes results from both the biological variability within biological replicas and the inherent technical noise. This strategy aims to substantially reduce both the positive and the negative false hits when using an arbitrary cut-off (e.g.: 1.5x) for the fold-change. CUT (Eq.1) adds correction for the groups of microarray spots probing redundantly the same gene.

$$CUT_i^{(PH)} = 1 + \left(\underbrace{\sqrt{\frac{r_i}{\chi^2(r_i;1-\varepsilon/2)}}}_{\text{chi-square correction}} + \sqrt{\frac{r_i}{\chi^2(r_i;\varepsilon/2)}} \right) \underbrace{\sqrt{\sum_{k=1}^{R_i} \left(\left(\frac{s_{ik}^{(PH)}}{\mu_{ik}^{(PH)}} \right)^2 + \left(\frac{s_{ik}^{(CO)}}{\mu_{ik}^{(CO)}} \right)^2 \right)}}_{\text{pooled CV}} \quad , \quad where: \tag{2}$$

$(PH) = (HO), (CM), (HM)$

$r_i = 4R_i - 1$ = number of degrees of freedom, R_i = number of spots probing the same gene i

χ^2 = chi-square score for r_i degrees of freedom and probability ε (=0.05) in this report

$s_{ik}^{(condition)}$ = standard deviation of gene i probed by spot k in the specified condition

$\mu_{ik}^{(condition)}$ = average expression of gene i probed by spot k in the specified condition

Profiling four biological replicates allows independent assessment of: i) average expression level, ii) expression variability and iii) expression coordination of each gene with each other individual gene. Combination of these measures was used to determine the remodeling of the topology and interplay of the functional genomic fabrics. The genomic fabric was defined by us as the most inter-coordinated and stably expressed gene network responsible for selected biological processes [31].

Pathway analysis: The genes pertaining to important functional pathways were selected from the maps developed by Kyoto Encyclopedia of Genes and Genomes (KEGG, www.kegg.jp; [32]). Particular attention was given to the genes involved in the oxidative phosphorylation (map 00190, ATPases, Cytochrome c oxidases, NADH dehydrogenases), chemokine signaling pathway (map 04062), vascular smooth muscle contraction (map 04270), mitochondrion ribosomal proteins and cell cycle (map 04110).

The corrected Weighted Pathway Regulation (WPR, [33] was used to quantify the transcriptomic effects of the three PH models on the selected functional pathways:

$$WPR_\Gamma^{(PH)} = \left\langle \mu_i^{(CO)} \underbrace{\left(\left| x_i^{(PH)} \right| - CUT_i^{(PH)} \right)}_{=0 \text{ if } \left| x_i^{(PH)} \right| < CUT_i^{(PH)}} \times \underbrace{\left(1 - p_i^{(PH)} \right)}_{\text{confidence of significant regulation}} \right\rangle_{\text{all } i \in \Gamma} \quad , \quad where: \text{ PH = CM, HO or HM} \tag{3}$$

$\langle A \rangle$ = median of A for all genes within the functional pathway Γ

$x_i^{(PH)}$ = fold-change (negative for down-regulation in the PH model with respect to CTR

$p_i^{(PH)}$ = p-value of the expression regulation of gene i in the PH model

WPR is more informative that the traditional percentage of regulated genes. WPR weights the contribution of each gene proportional to its normal (here in the CO group) average expression, absolute fold-change (until the cut-off accounting for the combined contributions of the technical noise and biological variability) and confidence of the expression regulation.

Like in previous experiments with kidneys [34] and hearts of mice subjected to chronic hypoxia [28, 35, 36], we computed the pair-wise Pearson correlation coefficient ρij between the expression levels of all pairs of expressed genes i and j in biological replicas of each condition. As speculated in previous papers [37, 38], strong expression correlation of two genes may represent a kind of "transcriptomic stoichiometry" aiming to optimize the pathway involving the encoded proteins. Expressions of (p-val < 0.05) statistically significantly synergistically expressed genes ($\rho ij > 0.950$) oscillate in phase (both genes increase and decrease their expression simultaneously), while expressions of antagonistically expressed genes ($\rho ij < -0.950$) manifest opposite tendencies (when one increases, the other decreases). Genes with $|\rho ij| < 0.025$ are considered as independently expressed. Different from the traditional cluster analysis that correlates the genes according to their similar behavior across various conditions or time points, we compute the correlation only between the expression levels in biological replicas of the same condition to determine "stoichiometric gene networks" [38].

The influence of a given gene i towards a particular pathway Γ was evaluated by its average coordination power (CP) against the expressions of the pathway Γ genes:

$$CP_{i;\Gamma}^{(condition)} = \left\langle \rho_{ij}^{(condition)} \right\rangle_{j\in\Gamma} \times 100/\% \quad (4)$$

CP takes values from -100% (all Γ- genes perfectly negatively correlated with gene i) to 100% (all Γ- genes perfectly positively correlated with gene i). A neutral gene towards that pathway has the CP close to zero, indicating that either almost all correlations are null or that the positives are balanced by the negatives.

Here, we introduce a new measure, termed Gene Pair Prominence (GPP), to quantify the relevance of gene interplays in each condition. The two genes can be from the same or from two different functional pathways. GPP takes values from -100% for the most prominent, negatively correlated genes to 100% for the most prominent, positively correlated genes in that condition. In order to simplify the landscape, GPP is considered zero for gene pairs whose absolute Pearson product-moment correlation coefficient between their expression levels in the four biological replicas of that condition was not significant ($|\rho_{ij}| < 0.950$).

$$GPP_{ij}^{(condition)} = \begin{cases} \dfrac{\mu_i^{(condition)} \rho_{ij}^{(condition)} \mu_j^{(condition)}}{\max\left|\mu_i^{(condition)} \rho_{ij}^{(condition)} \mu_j^{(condition)}\right|_{i\in\Gamma_1, j\in\Gamma_2}} \times 100\% & if \quad \left|\rho_{ij}^{(condition)}\right| > 0.950 \\ 0 & if \quad \left|\rho_{ij}^{(condition)}\right| < 0.950 \end{cases}, \quad where: \quad (5)$$

$\rho_{ij}^{(condition)}$ is the pair-wise Pearson correlation coefficient of the expression levels of genes $i \in \Gamma_1$, $j \in \Gamma_2$

condition = CO, HO, CM, HM; Γ_1, Γ_2 = functional pathways; $|X|$ = absolute value of X

3. Results

3.1. Decreased weight gain

The four-week weight gain in the control group was (204 ± 23) g. All PH groups had significantly lower weight gains as presented in Figure **1a**, the lowest was observed in MCT-treated rats exposed to hypoxia, i.e. group HM (WG = 33.6 ± 16.0)g.

3.2. Right ventricle hypertrophy

Figure **1b** presents the significant increase of the ratio between the right ventricle weight and the sum of the left ventricle and septum weights in the three PH models as normalized to the RV/(LV+S) in the control group. Note that right ventricle hypertrophy was statistically significant in all three experimental models.

3.3. Increased right ventricle systolic pressure

As depicted in Figure **1c**, RVSP was significantly increased in the hypoxia (HO) and MCT (CM) groups compared to the controls (CO). In the MCT + hypoxia group (HM), RVSP was further increased (significantly higher compared with HO and CM groups).

3.4. Histological alterations

Figures **1d-i** present H&E stained pulmonary arteries (42-101 μm) from the controls (**D**) and the experimental groups: HO (**e**), CM (**f**) and HM (**g**, **h**, **i**). Pulmonary arteries from CM and HO (show significant medial wall thickening compared with the control. The arteries from the HM group show further medial wall thickening, and (as seen in (**h**) and (**i**)), exhibit neointima formation and occlusion of the lumen.

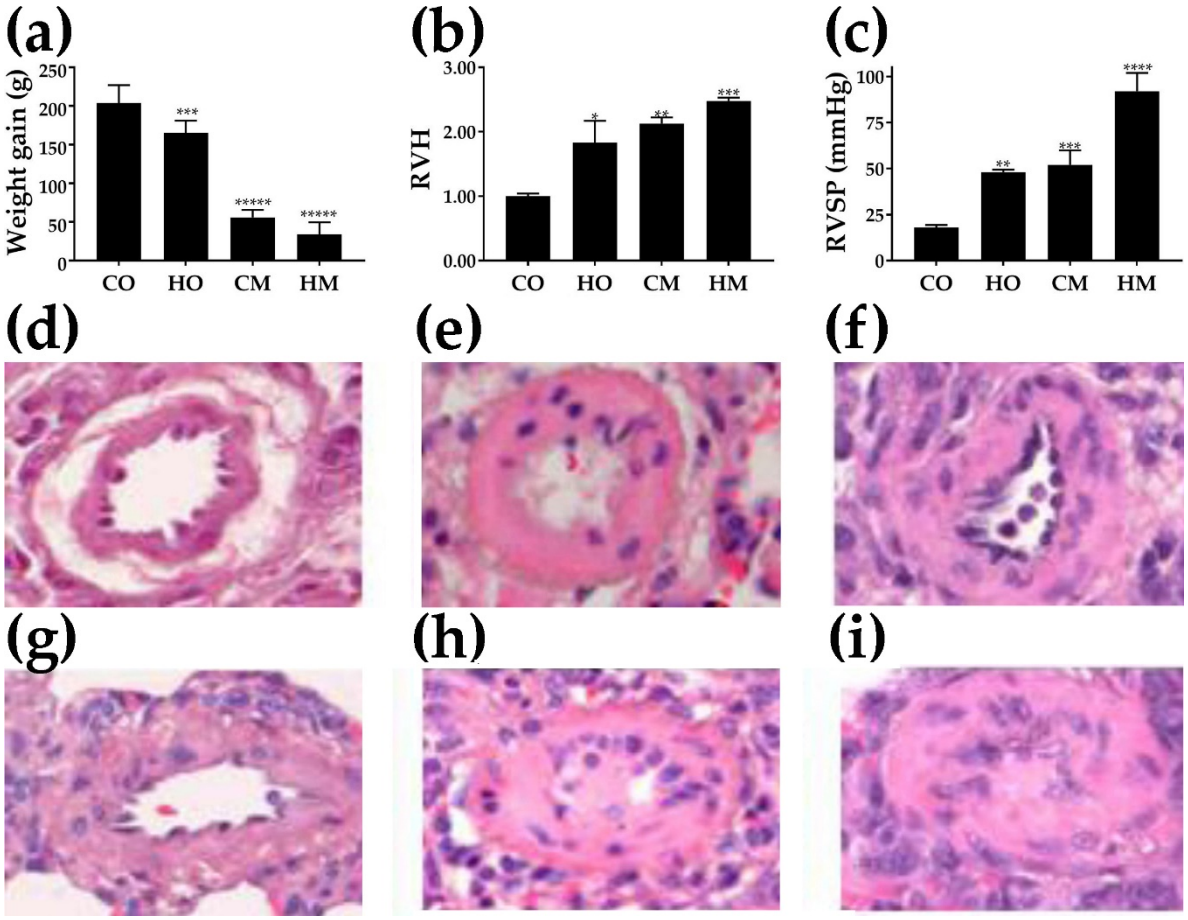

Figure 1: Effects of the pulmonary hypertension on: **(a)** weight gain, **(b**) right ventricle hypertrophy (RVH), **(c**) right ventricle systolic pressure (RVSP) and (**d-i**) histology of the pulmonary arteries. H&E stained sections from lungs of rats from the groups: CO (**d**), HO (**e**), CM (**f**), and HM (**g**, **h**, **i**). Note in (**h**) and (**i**) that the pulmonary arteries exhibit luminal obstruction. Statistical significance: * ($p < 0.05$), ** ($p < 0.01$), *** ($p < 0.005$), **** ($p < 0.001$)(https://www.medcalc.org/calc/comparison_of_means.php).

3.5. Overview of the transcriptomic alterations

Raw and processed gene expression results were deposited and are publicly available at https://www.ncbi.nlm.nih.gov/geo/query/acc.cgi?acc=GSE72707. Figures **2a** and **2b** indicate that all three experimental PH conditions regulated large numbers of genes and produced significant Weighted Pathway Regulation (WPR). The overall transcriptomic alterations (% of ALL REG and WPR) were consistent with the alterations in weight gain, RVH and RVSP data. Thus, MCT alone had a slightly larger effect than hypoxia alone; when MCT-treated rats were exposed to hypoxia, the alterations were substantially larger. Figure **2c** presents the WPR scores of some interesting groups of genes involved in respiration. Figure **2d** presents the significant fold-changes of genes whose regulation is often considered indicative for PH. Remarkably, in all three rat models of PH *Cav1* was overexpressed, by 13.18x in HO, 39.14x in CM and 79.06x in HM, substantially increased in the HM group. We found also that upregulation of *Cav1* is accompanied by the upregulation of *Nos3* (by 4.21x in HM) and upregulation of *Mmp2* (by 9.14x in HO, 33.59x in CM and 81.47x in HM group. The vast majority of the regulated genes by separate exposure to either hypoxia or MCT were altered in the same direction. However, as presented in Figure **2e**, few of them were oppositely regulated. Interestingly, when hypoxia and MCT are combined (as in HM), the regulation mostly follows the effects of the MCT exposure alone but with a larger fold-change.

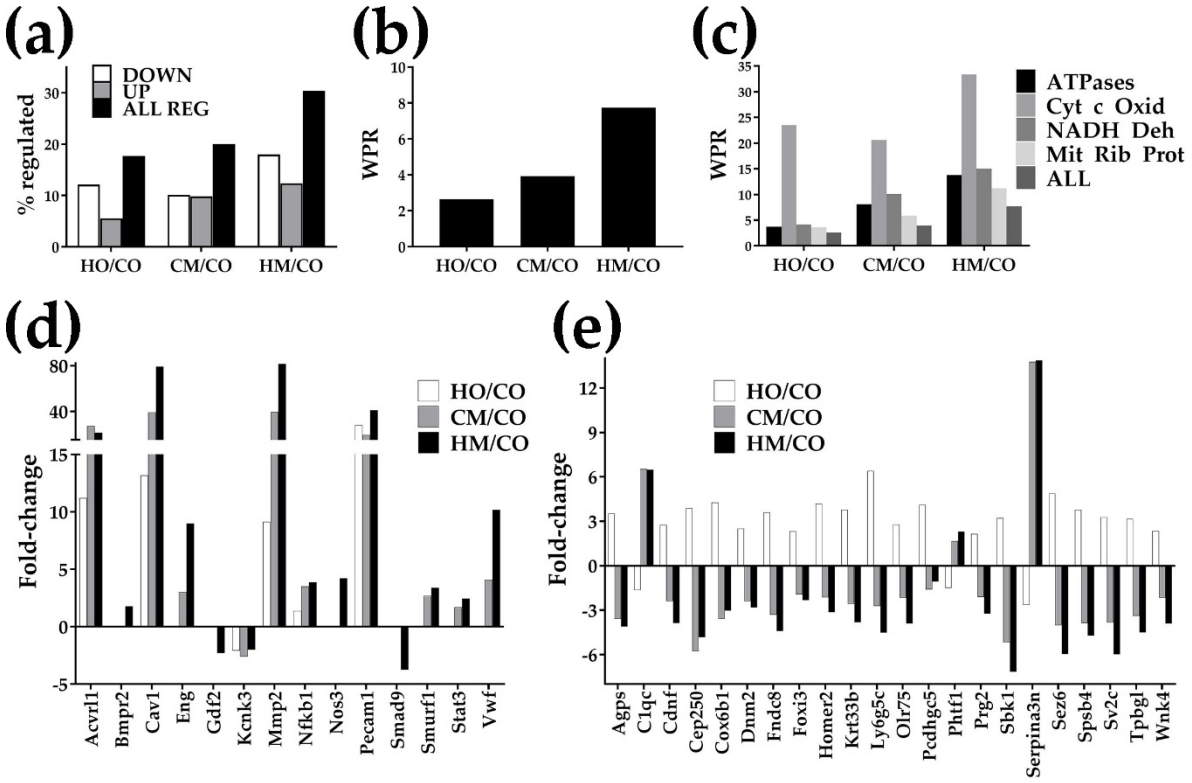

Figure 2: Transcriptomic alterations: (a) Number of regulated genes; (b) Weighted Pathway Regulation of all genes; (c) Weighted Pathway Regulation for some important groups of genes. Pathways: Cyt c Oxid = cytochrome c oxidases, **NADH Deh** = NADH dehydrogenases, **Mit Rib Prot** = mitochondrial ribosomal proteins. Note that **Cyt c Oxid** was by far the most altered group of respiratory genes. **HO/CO, CM/CO, HM/CO** = expression fold-change (negative for down-regulation) in the indicated comparison. **d) Statistically significant fold-changes of genes whose alterations are often considered as causing PH. Genes:** *Acvrl1* (Activin A receptor type II-like 1), *Bmpr2* (Bone morphogenetic protein receptor, type II (serine/threonine kinase)), *Cav1* (Caveolin 1, caveolae protein), *Eng* (Endoglin), *Gdf2* (Growth differentiation factor 2), *Kcnk3* (Potassium channel, subfamily K, member 3), *Mmp2* (Matrix metallopeptidase 2), *Nfkb1* (Nuclear factor NF-kappa-B p105 subunit), *Nos3* (Nitric oxide synthase 3, endothelial cell), *Pecam1* (Platelet/endothelial cell adhesion molecule 1), *Smad9* (SMAD family member 9), *Smurf1* (SMAD specific E3 ubiquitin protein ligase 1), *Stat3* (Signal transducer and activator of transcription 3 (acute-phase response factor)), *Vwf* (von Willebrand factor). **e) Significant opposite regulations. Genes:** *Agps* (alkylglycerone phosphate synthase), *C1qc* (complement component 1, q subcomponent, C chain), *Cdnf* (cerebral dopamine neurotrophic factor), *Cep250* (centrosomal protein 250), *Cox6b1* (cytochrome c oxidase subunit 6B1), *Dnm2* (dynamin 2), *Fndc8* (fibronectin type III domain containing 8), *Foxi3* (forkhead box I3), *Homer2* (homer homolog 2), *Krt33b* (keratin 33B), *Ly6g5c* (lymphocyte antigen 6 complex, locus G5C), *Olr75* (olfactory receptor 75), *Pcdhgc5* (protocadherin gamma subfamily C, 5), *Phtf1* (putative homeodomain transcription factor 1), *Prg2* (proteoglycan 2, bone marrow), *Sbk1* (SH3-binding domain kinase 1), *Serpina3n* (serine), *Sez6* (seizure related 6 homolog), *Spsb4* (splA/ryanodine receptor domain and SOCS box containing 4), *Sv2c* (synaptic vesicle glycoprotein 2c), *Tpbgl* (trophoblast glycoprotein-like), *Wnk4* (WNK lysine deficient protein kinase 4).

3.6. Regulation of the immune-inflammatory response

We found that PH regulated the expression of numerous genes involved in the (KEGG-determined map 04062) chemokine signaling pathway (Table 1). Table S1 in the Appendix presents other immune-inflammatory response genes (chemokines, cytokines, cytokine receptors, interferons, interleukins, and tumor necrosis factors) that were significantly regulated in at least one of the three rat PH models. Importantly, compared to the traditional standard of uniform 1.5x absolute fold-

change, our procedure to attach fold-change cut-offs to every single gene in each comparison identified additional regulated genes and eliminated false hits.

Gene	Description	HO/CO	CUT	CM/CO	CUT	HM/CO	CUT
Adcy2	Adenylate cyclase 2 (brain)	-4.24	2.32	-4.72	2.33	-4.21	2.34
Akt1	V-akt murine thymoma viral oncogene homolog 1	-1.42	1.61	1.09	1.94	1.80	1.78
Arrb1	Arrestin, beta 1	-9.55	2.86	-41.04	2.39	-52.82	2.53
Arrb2	Arrestin, beta 2	-1.38	2.11	3.37	2.54	2.95	2.24
Bcar1	Breast cancer anti-estrogen resistance 1	1.74	2.98	5.27	2.68	10.39	1.83
Ccl21	Chemokine (C-C motif) ligand 21	3.26	2.70	79.95	3.31	247.07	1.34
Ccl24	Chemokine (C-C motif) ligand 24	5.07	3.07	10.24	2.36	5.74	2.13
Ccl27	Chemokine (C-C motif) ligand 27	1.18	3.00	-7.76	1.85	-10.14	2.14
Ccl5	Chemokine (C-C motif) ligand 5	-1.35	1.85	4.56	2.45	4.40	1.65
Ccl6	C-C motif chemokine 6	7.53	3.32	22.93	2.72	38.26	1.98
Ccl9	Chemokine (C-C motif) ligand 9	-1.18	1.88	3.75	2.68	2.16	1.82
Ccr1l1	Chemokine (C-C motif) receptor 1-like 1	-1.48	1.46	-1.66	1.83	-2.77	1.80
Ccr9	Chemokine (C-C motif) receptor 9	4.01	2.84	10.35	2.65	1.29	1.78
Cx3cr1	Chemokine (C-X3-C motif) receptor 1	2.48	2.96	2.65	2.99	-2.53	2.35
Cxcl12	Chemokine (C-X-C motif) ligand 12	1.77	2.38	3.77	2.41	60.14	1.83
Cxcl3	Chemokine (C-X-C motif) ligand 3	1.61	2.33	3.93	3.13	3.33	1.93
Gnai2	Guanine nucleotide binding protein (G protein), alpha inhibiting 2	4.30	3.59	5.79	2.95	10.05	2.13
Gnb1	Guanine nucleotide binding protein (G protein), beta polypeptide 1	-4.22	2.37	-1.47	2.80	1.23	2.19
Gnb2	Guanine nucleotide binding protein (G protein), beta polypeptide 2	2.15	2.99	3.44	2.49	6.23	1.70
Gnb3	Guanine nucleotide binding protein (G protein), beta polypeptide 3	-3.33	2.17	-6.18	2.40	-11.78	2.42
Gng13	Guanine nucleotide binding protein (G protein), gamma 13	-2.64	2.43	-3.56	2.36	-2.33	2.10
Gng3	Guanine nucleotide binding protein (G protein), gamma 3	-22.18	2.46	-21.14	2.51	-32.06	2.44
Gng4	guanine nucleotide binding protein (G protein), gamma 4 subunit	-1.24	1.46	-1.29	1.77	-2.19	1.71
Gngt2	Guanine nucleotide binding protein (G protein), gamma transducing activity polypeptide 2	1.76	2.62	7.16	2.75	11.11	1.63
Grb2	Growth factor receptor bound protein 2	4.31	2.79	3.69	2.75	6.32	1.87
Grk6	G protein-coupled receptor kinase 6	-3.00	2.59	-1.04	2.69	1.69	2.07
Gsk3a	Glycogen synthase kinase 3 alpha	-4.67	2.17	-4.44	2.31	-7.27	2.21
Mapk3	Mitogen activated protein kinase 3	1.72	2.92	-3.71	2.05	-3.42	1.89
Nfkbia	Nuclear factor of kappa light polypeptide gene enhancer in B-cells inhibitor, alpha	1.92	3.60	5.56	3.03	9.00	2.20
Nfkbid	NFKB inhibitor delta	-1.79	1.64	-2.08	1.89	-3.25	1.85
Pak1	P21 protein (Cdc42/Rac)-activated kinase 1	-1.79	2.19	-3.31	2.17	-3.17	2.15
Pik3r1	Phosphoinositide-3-kinase, regulatory subunit 1 (alpha)	1.20	2.03	2.77	2.28	4.25	1.28
Pik3r5	Phosphoinositide-3-kinase, regulatory subunit 5	-11.53	2.66	-5.87	2.40	-7.66	2.38
Plcb4	Phospholipase C, beta 4	3.18	2.86	6.70	2.99	-4.79	2.12
Ppbp	Pro-platelet basic protein (chemokine (C-X-C motif) ligand 7)	-1.05	1.41	-1.16	2.11	-3.06	2.13
Ptk2b	PTK2B protein tyrosine kinase 2 beta	-12.47	2.45	-6.89	2.36	-8.51	2.34
Rap1b	RAP1B, member of RAS oncogene family	-3.04	2.84	-1.84	3.17	-1.17	2.37
Rela	V-rel reticuloendotheliosis viral oncogene homolog A (avian)	-3.38	2.07	-1.15	2.29	1.22	1.98
Rhoa	Ras homolog gene family, member A	7.00	2.80	6.78	2.52	9.21	1.24
Shc1	SHC (Src homology 2 domain containing) transforming protein 1	-2.71	2.09	-4.11	2.03	-4.94	2.08
Sos1	Son of sevenless homolog 1 (Drosophila)	1.02	1.99	2.07	2.49	-2.86	1.77
Tiam1	T-cell lymphoma invasion and metastasis 1	-2.79	1.75	-2.67	2.13	-4.85	1.95
Vav2	Vav 2 guanine nucleotide exchange factor	2.06	2.74	3.44	2.43	6.02	1.45
Xcl1	Chemokine (C motif) ligand 1	-1.51	1.96	-1.53	2.20	-3.49	2.03

Table 1: Regulation of the chemokine signaling pathway (KEGG, map rno04062) genes. Significant (larger than CUT) absolute fold-changes are in red background for up-regulated and green background for down-regulated. Note the range of the CUTs, from 1.24 (for the regulation of *Rhoa* in HM vs CO) to 3.60 (for the regulation of *Nfkbia* in HO vs. CO). Our procedure to determine the cut-off for the absolute fold-change for every gene in each comparison instead of using a fixed cut-off (like 1.5x) identified additional regulated genes (CUT in yellow background, e.g. *Ccr1l1* in HO/CO). It also eliminated the false regulations (expression ratio in grey background, e.g. *Bcar1* in HO/CO) whose absolute (although over 1.5x) fold-change) was below the CUT (2.98) computed for that gene in the compared conditions.

3.7. Regulation of the vascular smooth muscle contraction pathway

Figure 3 presents the regulation of the 122 quantified genes involved in the (KEGG-determined map 04270, www.kegg.jp) vascular smooth muscle contraction pathway in the three PH models. Note the substantially increased number of regulated genes when the MCT-treated rats were exposed to hypoxia (30% up + 49% down, Fig. **3a**) compared to when they were exposed to only hypoxia (16%

up + 14% down, Fig. **3b**) or treated with MCT (26% up + 16% down, Fig. **3c**). The percentages of all regulated genes in this pathway (30% in HO, 42% in CM and 79% in HM) were significantly larger than the percentages of all regulated genes in the entire transcriptome (18% in HO, 20% in CM and 30% in HM) as illustrated in Fig. 2a.

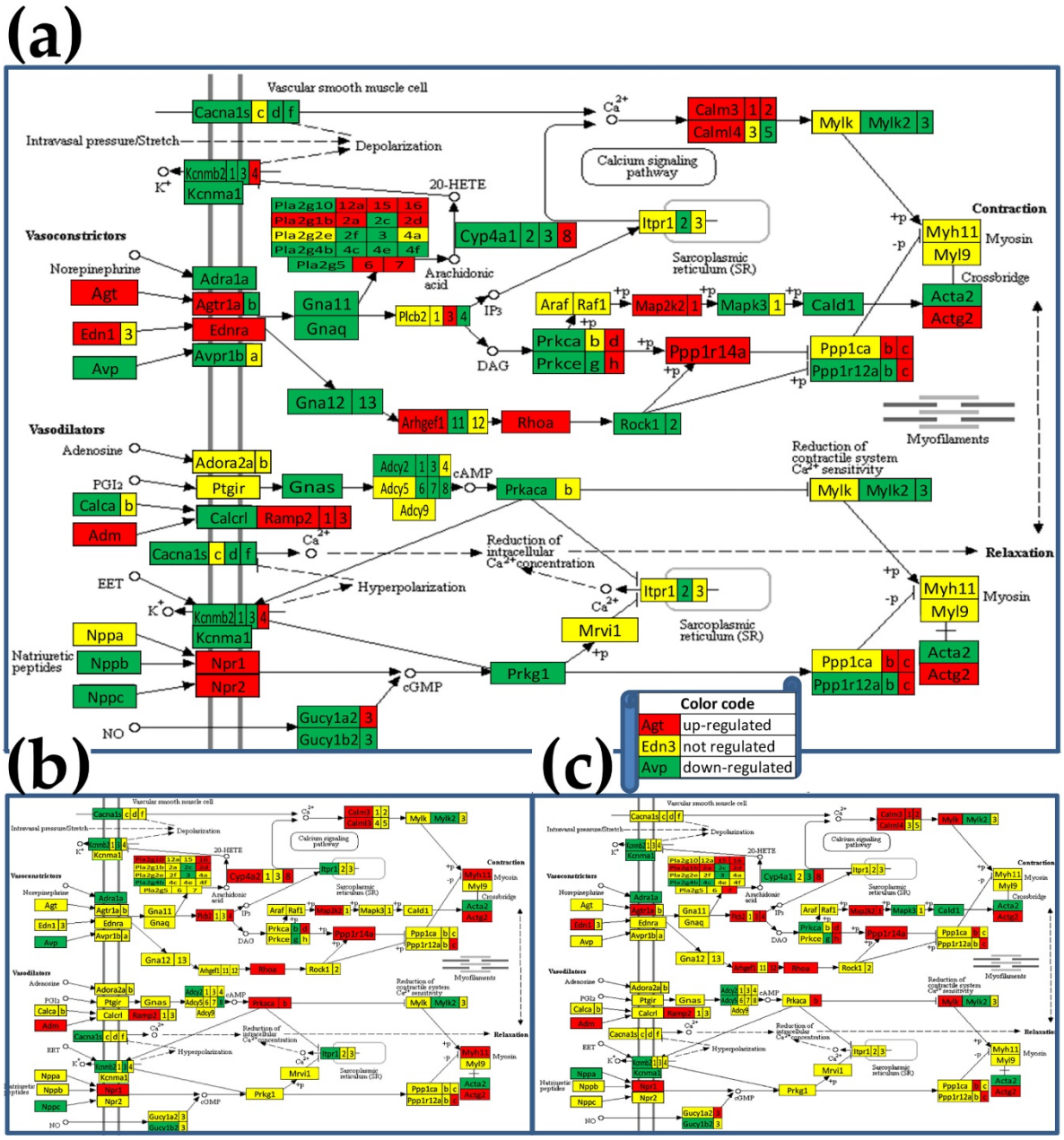

Figure 3: Regulation of the vascular smooth muscle contraction pathway. (a) Rats treated with MCT and exposed to hypoxia (HM); **(b)** Rats exposed to only hypoxia (HO); **(c)** Rats treated with monocrotaline only (CM). **Regulated genes:** *Acta2* (smooth muscle alpha-actin), *Actg2* (actin, gamma 2, smooth muscle, enteric), *Adcy2* (adenylate cyclase 2), *Adora2a* (adenosine A2a receptor), *Agtr1a* (angiotensin II receptor, type 1a), *Ang* (angiogenin), *Araf* (v-raf murine sarcoma 3611 viral oncogene homolog), *Avp* (arginine vasopressin), *Cacna1d/s* (calcium channel, voltage-dependent, L type, alpha 1D/S subunit), *Cald1* (caldesmon 1), *Calm2* (calmodulin 2), *Cyp4a1/8* (cytochrome P450, family 4, subfamily a, polypeptide 1/8), *Gnas* (GNAS complex locus), *Gucy1b2* (guanylate cyclase 1, soluble, beta 2), *Itpr1* (inositol 1,4,5-trisphosphate receptor, type 1), *Kcnmb2* (potassium large conductance calcium-activated channel, subfamily M, beta member 2), *Map2k2* (mitogen activated protein kinase kinase 2), *Mapk3* (mitogen activated protein kinase 3), *Myl9* (myosin, light chain 9, regulatory), *Mylk2*

(myosin light chain kinase 2), *Npr1/2* (natriuretic peptide receptor guanylate cyclase A/B), *Pla2g1b* (phospholipase A2, group IB, pancreas), phospholipases A2 (*Pla2g2d*, *Pla2g3*, *Pla2g4b*, *Pla2g6*), *Plcb4* (phospholipase C, beta 4), *Ppp1ca* (protein phosphatase 1, catalytic subunit, alpha isozyme), *Ppp1r12c/14a/14b* (protein phosphatase 1, regulatory subunit 12C/14A/14B), *Prkca/e* (protein kinase C, alpha/epsilon), *Ptgir* (prostaglandin I2 (prostacyclin) receptor (IP)), *Raf1* (v-raf-leukemia viral oncogene 1), *Ramp1/3* (receptor (G protein-coupled) activity modifying protein 1/3), *Rhoa* (ras homolog family member A).

3.8. Regulation of the cell-cycle pathway

Figure 4 presents the regulation of the 112 quantified genes responsible for the (KEGG-determined map 04110, www.kegg.jp) cell-cycle pathway in the three PH models with respect to control. As expected, many more genes were regulated in the lungs of MCT-treated rats exposed to hypoxia (36% up + 42% down, Fig. 4**a**) than in those of rats exposed to only hypoxia (7% up + 16% down, Fig. 4**b**) or treated with monocrotaline alone (25% up + 11% down, Fig. 4**c**). Of note are the much higher percentages of regulated genes in the cell-cycle pathway (23% in HO, 36% in CM and 78% in HM) than the percentages of regulated genes in the entire transcriptome (18% in HO, 20% in CM and 30% in HM) as illustrated in Fig. 2a.

Genes were regulated in both DNA replication phase (**S**) and mitosis phase (**M**), as well as during the temporal separation gaps (denoted by **G1** and **G2** in Fig. **4a**). Interestingly, all components of the minichromosome maintenance complex (*Mcm*) were regulated in MCT-treated rats exposed to hypoxia, with down-regulation of *Mcm3* and up-regulation of *Mcm7* consistent in the other two PH groups. In contrast, while no subunit of the origin recognition complex (*Orc*) was regulated by MCT administration and only *Orc4* was down-regulated by hypoxia, when MCT-treated animals were exposed to hypoxia, all but *Orc4 Orc* subunits were regulated.

Preprints (www.preprints.org) | NOT PEER-REVIEWED | Posted: 21 December 2019 doi:10.20944/preprints201912.0280.v1

Peer-reviewed version available at Genes 2020, 11, 126; doi:10.3390/genes11020126

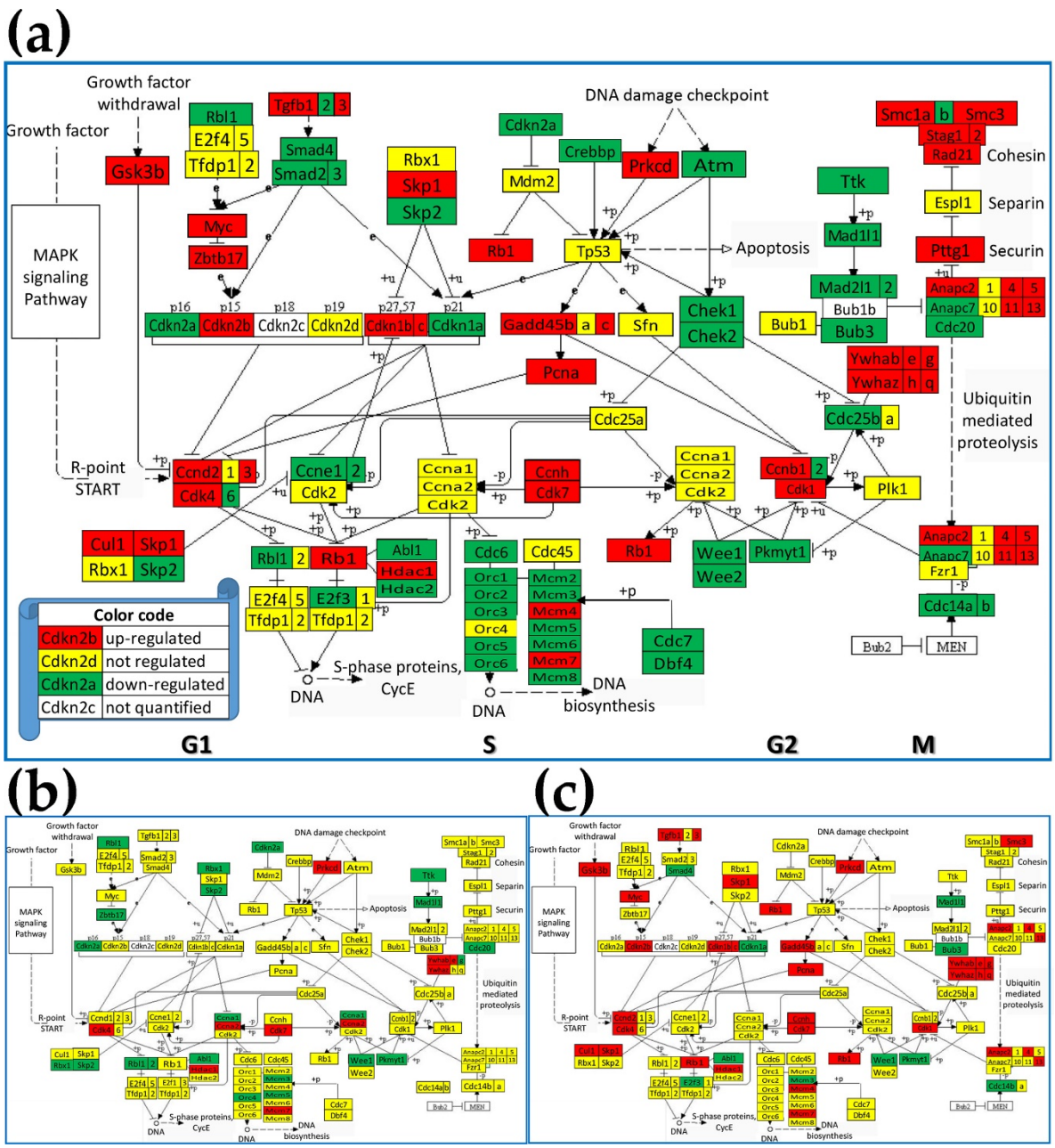

Figure 4: Regulation of the cell-cycle pathway. (a) Rats treated with MCT and exposed to hypoxia (HM); **(b)** Rats exposed to only hypoxia (HO); **(c)** Rats treated with monocrotaline only (CM). **Regulated genes:** *Abl1* (C-abl oncogene 1, non-receptor tyrosine kinase), subunits of the anaphase promoting complex (*Anapc2, Anapc4, Anapc5, Anapc7, Anapc11, Anapc13*), *Atm* (ataxia telangiectasia mutated homolog), *Bub3* (budding uninhibited by benzimidazoles 3 homolog), cyclins (*Ccnb1, Ccnb2, Ccnd2, Ccnd3, Ccne1, Ccne2, Ccnh*), cell division cycles (*Cdc14a, Cdc14b, Cdc20, Cdc25a, Cdc25b, Cdc6*), cyclin-dependent kinases (*Cdk1, Cdk4, Cdk6, Cdk7*), cyclin-dependent kinase inhibitors (*Cdkn1a, Cdkn1b, Cdkn1c, Cdkn2a, Cdkn2b*), checkpoint kinases (*Chek1, Chek2*), *Cul1* (culin 1), *Dbf4* (DBF4 homolog), *Gsk3b* (Glycogen synthase kinase 3 beta), *E2f3* (E2F transcription factor 3), growth arrest and DNA-damage-inducibles (*Gadd45b, Gadd45c*), histone deacetylases (*Hdac1, Hdac2*), MAD2 mitotic arrest deficient-likes (*Mad2l1, Mad2l2*), components of the minichromosome maintenance complex (*Mcm2, Mcm3, Mcm4, Mcm5, Mcm6, Mcm7, Mcm8*), *Myc* (myelocytomatosis oncogene), subunits of the origin recognition complex (*Orc1, Orc2, Orc3,, Orc4, Orc5, Orc6*), *Pcna* (proliferating cell nuclear antigen), *Pkmyt1* (protein kinase, membrane associated tyrosine/threonine 1), *Prkcd* (protein kinase C, delta), *Rad21* (RAD21 homolog), retinoblastomas (*Rb1, Rbl1*), *Skp1/2* (S-phase kinase-associated protein 1/2), structural maintenance of chromosomes (*Smc1a, Smc1b, Smc3*), SMAD family members

(*Smad2*, *Smad3*, *Smad4*), stromal antigens (*Stag1*, *Stag2*), transforming growth factors beta (*Tgfb1*, *Tgfb2*, *Tgfb3*), *Wee1* (WEE1 G2 checkpoint kinase), *Wee2* (oocyte meiosis inhibiting kinase), tyrosine 3-monooxygenase/tryptophan 5-monooxygenase activation proteins (*Ywhab*, *Ywhae*, *Ywhag*, *Ywhah*, *Ywhaq*, *Ywhaz*), *Zbtb17* (zinc finger and BTB domain containing 17).

3.9. Alteration of the cellular respiration

A particular attention was given to the regulation of the major groups of genes involved in the oxidative phosphorylation: ATPases, cytochrome c oxidases and NADH dehydrogenases (Table 2). As illustrated In Fig. 2c, the Weighted Pathway Regulation (WPR) score revealed that these groups of genes were altered much more than the entire transcriptome. Alteration of the genes encoding mitochondrial ribosomal proteins is also presented for comparison in the Appendix Table S2.

Preprints (www.preprints.org) | NOT PEER-REVIEWED | Posted: 21 December 2019 doi:10.20944/preprints201912.0280.v1

Peer-reviewed version available at Genes 2020, 11, 126; doi:10.3390/genes11020126

Gene	Description	HO/CO	CUT	CM/CO	CUT	HM/CO	CUT
Atp11b	ATPase phospholipid transporting 11B	-1.74	2.28	1.34	2.46	2.05	1.82
Atp13a2	ATPase type 13A2	-1.67	2.18	1.55	2.40	2.11	2.00
Atp1a1	ATPase, Na+/K+ transporting, alpha 1 polypeptide	-1.78	3.34	4.01	3.08	6.65	2.25
Atp1a3	ATPase, Na+/K+ transporting, alpha 3 polypeptide	-1.52	1.71	-1.86	1.95	-3.48	2.07
Atp1b2	ATPase, Na+/K+ transporting, beta 2 polypeptide	-146.48	3.21	-257.37	2.51	-111.20	2.47
Atp1b3	ATPase, Na+/K+ transporting, beta 3 polypeptide	2.14	2.32	12.00	2.35	15.88	1.26
Atp2a2	ATPase, Ca++ transporting, cardiac muscle, slow twitch 2	1.56	2.48	4.83	2.46	10.66	1.49
Atp2a3	ATPase, Ca++ transporting, ubiquitous	1.40	1.95	1.62	1.87	1.88	1.39
Atp2b1	ATPase, Ca++ transporting, plasma membrane 1	-3.70	3.00	-1.19	2.86	1.30	2.34
Atp2b4	ATPase, Ca++ transporting, plasma membrane 4	-2.48	1.90	-1.69	2.59	-11.70	2.28
Atp2c1	ATPase, Ca++ transporting, type 2C, member 1	-1.35	1.67	1.24	1.69	1.85	1.50
Atp4a	ATPase, H+/K+ exchanging, alpha polypeptide	1.13	1.59	-1.12	1.94	-2.35	1.61
Atp5d	ATP synthase, H+ transporting, mitochondrial F1 complex, delta sub	2.27	3.21	6.84	2.82	9.15	1.92
Atp5f1	ATP synthase, H+ transporting, mitochondrial Fo complex, subunit I	4.36	3.01	27.45	2.92	51.30	1.67
Atp5g1	ATP synthase, H+ transporting, mitochondrial Fo complex, subunit C	4.71	3.18	10.84	2.78	16.08	2.08
Atp5g2	ATP synthase, H+ transporting, mitochondrial Fo complex, subunit C	3.21	2.91	14.44	2.84	26.97	1.86
Atp5g3	ATP synthase membrane subunit c locus 3	-7.56	3.23	-1.08	3.22	1.35	2.35
Atp5i	ATP synthase, H+ transporting, mitochondrial Fo complex, subunit I	17.18	2.97	11.45	2.89	15.65	2.19
Atp5j2	ATP synthase, H+ transporting, mitochondrial Fo complex, subunit I	-1.27	2.91	5.30	2.90	8.37	2.24
Atp6v0a1	ATPase, H+ transporting, lysosomal V0 subunit A1	4.14	2.57	3.11	2.35	4.83	1.65
Atp6v0a2	ATPase, H+ transporting, lysosomal V0 subunit A2	-2.76	2.21	-2.35	2.37	-1.52	2.16
Atp6v0b	ATPase, H+ transporting, lysosomal V0 subunit B	-6.71	3.10	-1.45	3.18	-1.31	2.59
Atp6v0c	ATPase, H+ transporting, lysosomal V0 subunit C	-31.61	2.78	-5.37	3.13	-3.65	2.39
Atp6v0e1	ATPase, H+ transporting, lysosomal, V0 subunit e1	1.78	2.25	16.44	2.87	26.14	1.32
Atp6v0e2	ATPase, H+ transporting V0 subunit e2	1.84	2.59	-3.40	1.79	-5.62	1.95
Atp6v1f	ATPase, H transporting, lysosomal V1 subunit F	1.10	2.22	5.42	2.78	9.44	1.53
Atp6v1g2	ATPase, H+ transporting, lysosomal V1 subunit G2	-11.80	2.62	-16.92	2.68	-39.54	2.66
Atp7b	ATPase, Cu++ transporting, beta polypeptide	-1.10	1.95	-1.61	2.13	-4.23	1.93
Atpif1	ATPase inhibitory factor 1	1.06	3.10	5.02	3.13	8.16	2.21
Cox14	cytochrome c oxidase assembly factor COX14	-3.02	2.38	1.25	2.48	1.45	2.12
Cox17	cytochrome c oxidase assembly homolog 17	-1.43	3.42	2.09	3.07	3.01	2.28
Cox18	cytochrome c oxidase assembly homolog 18	-2.41	2.11	-1.51	2.20	-1.23	2.03
Cox4i1	cytochrome c oxidase subunit IV isoform 1	11.99	2.91	30.01	2.81	52.39	1.89
Cox4i2	cytochrome c oxidase subunit IV isoform 2 (lung)	-6.30	3.02	-4.07	2.77	-2.89	2.32
Cox5b	cytochrome c oxidase subunit Vb	-9.14	2.93	-1.85	3.15	-1.02	2.34
Cox6a1	cytochrome c oxidase, subunit VIa, polypeptide 1	-1.85	3.68	1.66	3.10	2.87	2.24
Cox6a2	cytochrome c oxidase subunit VIa polypeptide 2	1.33	2.05	2.99	2.60	16.89	2.29
Cox6b1	cytochrome c oxidase subunit 6B1	4.27	2.82	-3.59	2.54	-3.02	2.29
Cox6b2	cytochrome c oxidase subunit VIb polypeptide 2	-3.95	2.64	-7.82	2.34	-7.12	2.32
Cox6c	cytochrome c oxidase, subunit VIc	4.56	3.49	11.35	2.92	18.57	2.02
Cox7a2	cytochrome c oxidase subunit VIIa polypeptide 2	1.85	2.97	7.68	2.74	12.31	1.95
Cox7b	cytochrome c oxidase subunit VIIb	1.50	2.03	6.58	2.77	11.58	1.79
Cox8a	cytochrome c oxidase subunit VIIIa	-4.07	3.07	1.27	3.18	2.50	2.33
Cox8b	cytochrome c oxidase, subunit VIIIb	2.96	2.01	2.35	1.93	6.01	2.37
Coa5	cytochrome C oxidase assembly factor 5	-20.24	2.92	-8.03	3.05	-11.72	2.93
Ndufa10	NADH dehydrogenase (ubiquinone) 1 alpha subcomplex 10	1.24	2.99	1.81	2.56	3.27	1.92
Ndufa11	NADH dehydrogenase (ubiquinone) 1 alpha subcomplex 11	-1.02	2.24	3.51	2.08	3.92	1.72
Ndufa13	NADH:ubiquinone oxidoreductase subunit A13	-2.20	3.07	3.05	3.10	5.35	2.18
Ndufa3	NADH dehydrogenase (ubiquinone) 1 alpha subcomplex, 3	-4.15	2.81	-2.79	2.51	-2.08	2.25
Ndufa6	NADH dehydrogenase (ubiquinone) 1 alpha subcomplex, 6 (B14)	4.42	3.33	15.50	2.84	28.28	1.71
Ndufaf5	NADH dehydrogenase (ubiquinone) complex I, assembly factor 5	-1.16	2.21	1.50	2.45	2.21	1.94
Ndufb10	NADH dehydrogenase (ubiquinone) 1 beta subcomplex, 10	2.67	3.13	4.78	2.67	7.57	1.63
Ndufb2	NADH dehydrogenase (ubiquinone) 1 beta subcomplex, 2	7.38	3.22	20.76	2.78	35.55	1.73
Ndufb3	NADH dehydrogenase (ubiquinone) 1 beta subcomplex 3	3.15	2.92	7.29	2.42	12.14	1.60
Ndufb4	NADH dehydrogenase (ubiquinone) 1 beta subcomplex 4	3.52	3.35	11.33	2.85	21.34	1.89
Ndufb5	NADH dehydrogenase (ubiquinone) 1 beta subcomplex, 5	1.31	2.83	4.31	2.77	6.50	1.94
Ndufb6	NADH dehydrogenase (ubiquinone) 1 beta subcomplex, 6	-6.75	2.75	-1.20	3.14	1.33	2.28
Ndufb7	NADH dehydrogenase (ubiquinone) 1 beta subcomplex, 7	-4.28	3.63	-1.59	3.12	-1.12	2.32
Ndufb8	NADH dehydrogenase (ubiquinone) 1 beta subcomplex 8	2.64	3.37	7.96	3.09	13.61	2.35
Ndufb9	NADH dehydrogenase (ubiquinone) 1 beta subcomplex, 9	1.67	2.89	11.81	2.95	19.58	2.16
Ndufs3	NADH dehydrogenase (ubiquinone) Fe-S protein 3	-5.54	3.14	-1.39	3.14	1.08	2.42
Ndufs5	NADH dehydrogenase (ubiquinone) Fe-S protein 5	3.54	2.87	12.91	2.84	23.34	1.94
Ndufs7	NADH dehydrogenase (ubiquinone) Fe-S protein 7	5.04	3.35	8.90	2.68	10.68	1.74
Ndufv1	NADH dehydrogenase (ubiquinone) flavoprotein 1	5.55	3.38	8.51	2.82	14.54	1.94
Ndufv3	NADH dehydrogenase (ubiquinone) flavoprotein 3	1.32	1.95	2.12	2.22	3.71	1.24
Sdhaf2	succinate dehydrogenase complex assembly factor 2	2.15	2.69	4.59	2.76	7.66	1.73

373

Table 2: Significantly up (red background) and down (negative fold-change, green background) regulated ATPases, cytochrome c oxidases and NADH dehydrogenases in the three PH rat models. Note the range of the CUTs, from 1.24 (for the regulation of *Ndufv3* in HM vs CO) to 3.68 (for the regulation of *Cox6a1* in HO vs. CO). Our procedure to determine the cut-off for the absolute fold-change for every gene in each comparison instead of using a fixed cut-off (like 1.5x) eliminated the false regulations (expression ratio in grey background, e.g. *Atp11b* in HO/CO) whose absolute (although over 1.5x) fold-change) was below the CUT (2.28) computed for that gene in the compared conditions.

3.10. Remodeling of the relationship between the genes involved in the vascular smooth muscle contraction and the oxidative phosphorylation

We studied how much the interaction of the vascular smooth muscle contraction genes (VSMC, https://www.kegg.jp/pathway/rno04270) (presented in Fig. 3) with genes involved in the oxidative phosphorylation (OP), particularly with the ATPases is remodeled by the pulmonary hypertension. For this, we computed the Pearson correlation coefficients for the 1,248 pairs that can be formed with the 32 ATPases and 39 VSMC genes adequately quantified in each of the four experimental conditions. Interestingly, we found that each PH condition significantly reduced the net positive correlation (i.e. number of positively (p) – number of negatively (n) correlated gene-pairs): from 450 (= 472p – 22n) in CO to 236 (= 280p – 44n) in HO, 340 (= 455p – 115n) in CM and 208 (= 262p – 54n) in HM. Fig. 5 presents the significantly synergistically, antagonistically and independently expressed pairs of VSMC genes with ATPases in CO and the pairs whose expression correlation was significantly altered in the three PH models.

Preprints (www.preprints.org) | NOT PEER-REVIEWED | Posted: 21 December 2019 doi:10.20944/preprints201912.0280.v1

Peer-reviewed version available at Genes 2020, 11, 126; doi:10.3390/genes11020126

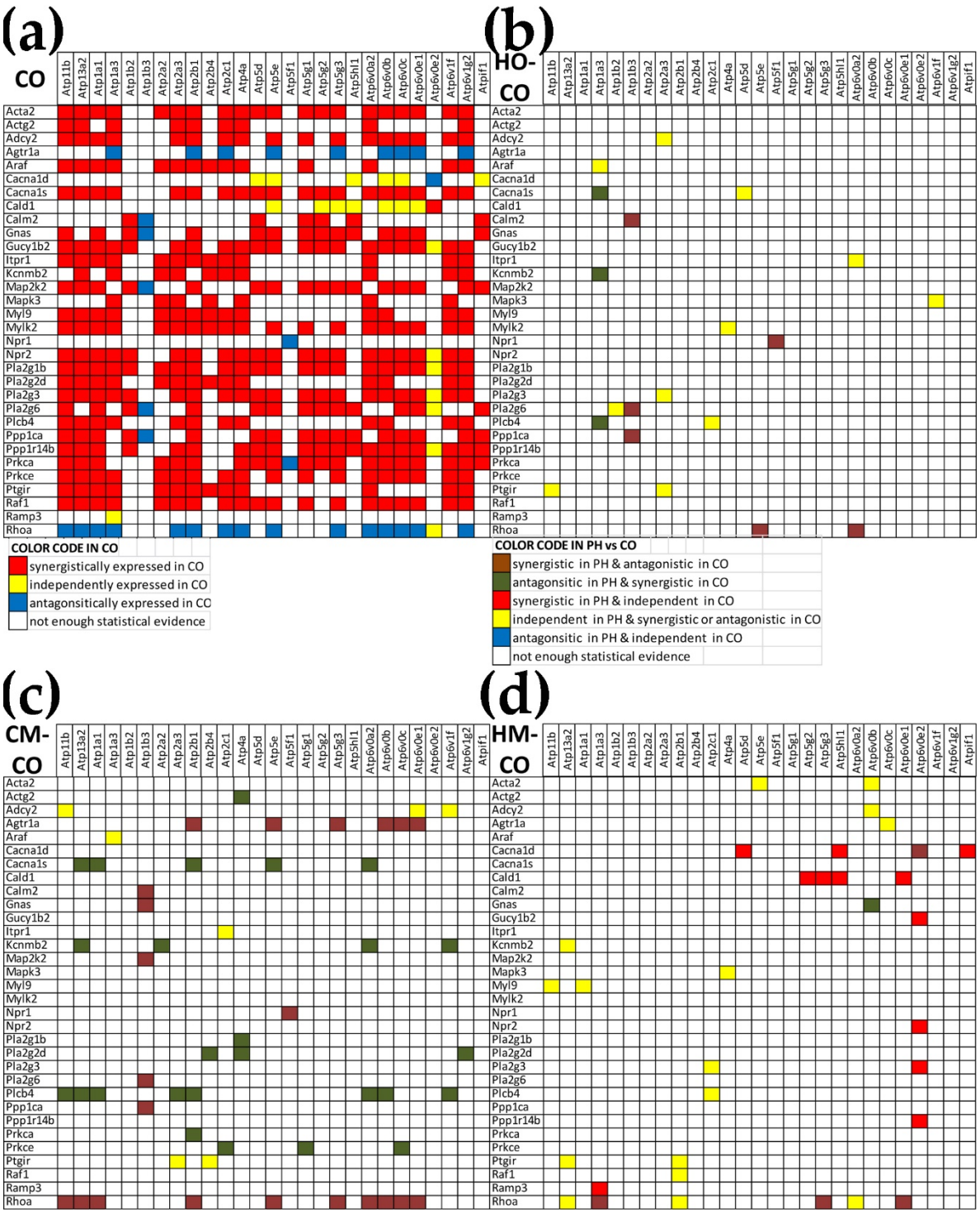

Figure 5: Synergistically (red squares), antagonistically (blue squares) and independently (yellow squares) expressed pairs of VSMC genes and ATPases in CO (**a**) whose expression correlation was significantly altered by hypoxia (**b**), monocrotaline (**c**) or the combined action of hypoxia and monocrotaline (**d**). A blank square in (**a**) indicates that the correlation is not ($p < 0.05$) statistically significant.

We then used the new measure Gene Pair Prominence (GPP, Eq. 4) to rank the gene-pairs of the interplay between the two groups of genes. The positive and negative GPPs were plotted separately (as CO+ and CO-, HO+ and HO-, CM+ and CM-, HM+ and HM-) to emphasize the type and importance of their expression correlation. The GPPs of all genes in each condition was expressed as the percentage of the maximal absolute GPP in that condition, regardless if it was positive or negative.

Preprints (www.preprints.org) | NOT PEER-REVIEWED | Posted: 21 December 2019 doi:10.20944/preprints201912.0280.v1

Peer-reviewed version available at Genes 2020, 11, 126; doi:10.3390/genes11020126

Excepting in the CM condition, where the genes of the dominant pair (*Cyp4a8-Atp5e*) were negatively correlated, the positively correlated pairs have much larger GPPs than the negatively correlated ones, meaning that expression of most ATPases oscillates in phase with most VSMC genes.

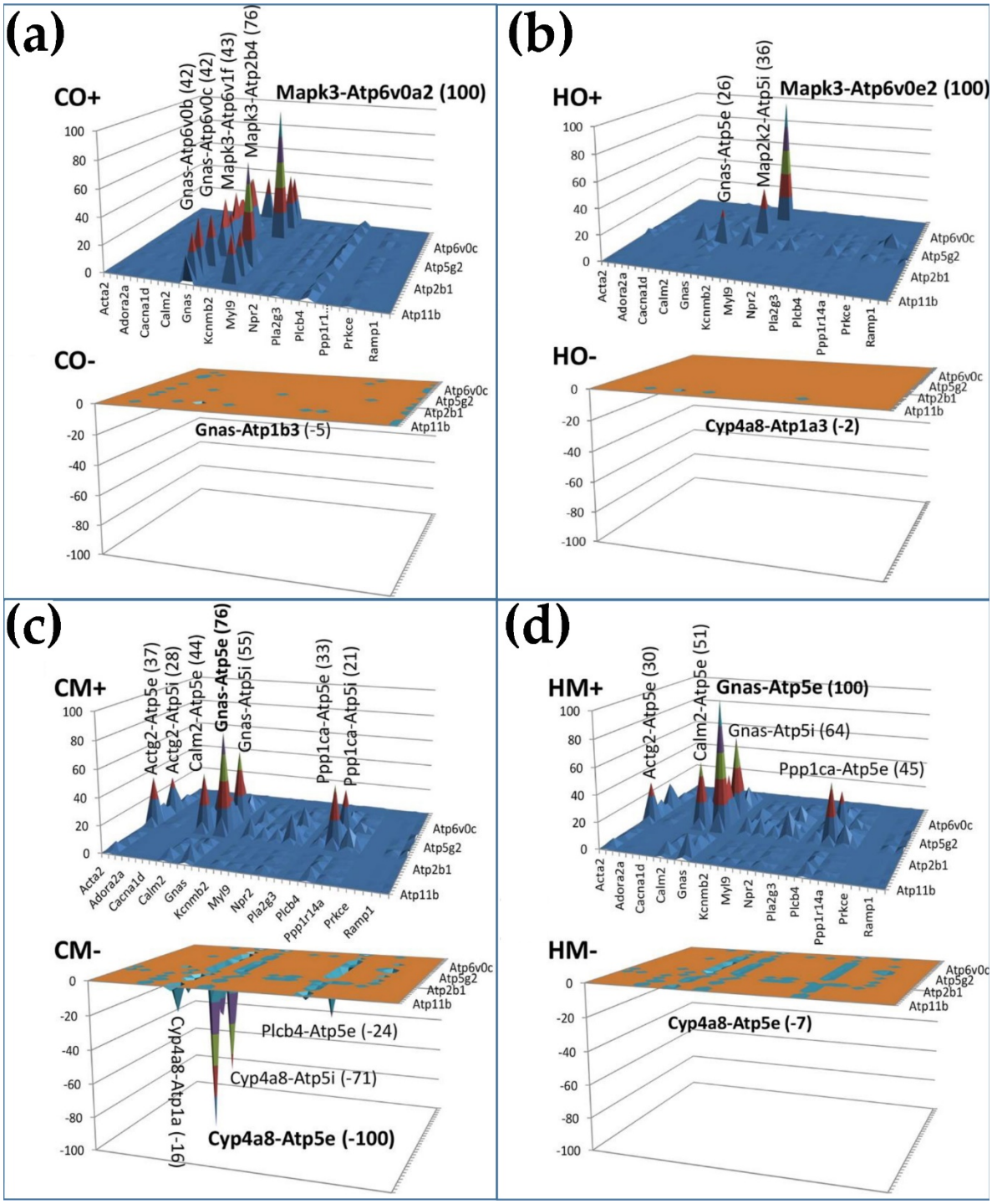

Figure 6: Gene Pair Prominence (GPP) analysis of the interaction of vascular smooth muscle contraction genes with the ATPases in the four conditions. **(a)** GPP values for the 472 positively ($\varrho > 0.9$) and 36 negatively ($\varrho < -0.9$) correlated gene-pairs in CO; **(b)** GPP values for the 280 positively and 4 negatively correlated gene-pairs in HO; **(c)** GPP values for the 455 positively and 115 negatively correlated gene-pairs in CM; **(d)** GPP values for the 262 positively and 4 negatively correlated gene-pairs in HM.

The analysis pointed out three remarkable H^+ transporters (*Atp5e, Atp6v0a2, Atp6v0e2*) in strong partnership with three VSMC genes: *Cyp4a8* (cytochrome P450 family 4, subfamily a, polypeptide 8), *Gnas* (GNAS complex locus) and *Mapk3* (mitogen activated protein kinase 3). *Mapk3*, involved in a wide range of pathways (listed in https://www.ncbi.nlm.nih.gov/gene/50689), provides the most prominent positive pairs with *Atp6v0a2* in normal atmospheric conditions and with *Atp6v0e2* in hypoxia (obtained by reducing the atmospheric pressure in half).

4. Discussion

We examined the transcriptomic alterations in the right lungs of male rats with pulmonary hypertension induced by exposure to hypoxia (HO group), administration of monocrotaline (CM group), or exposure to hypoxia of monocrotaline-treated animals (HM group). There are numerous common features of the three experimental groups, making them valuable models for the human pulmonary hypertension, including lower weight gain but right ventricle hypertrophy and increased right ventricle systolic pressure. However, there are also significant differences as revealed by the present and previous studies.

At 4 weeks after hypobaric hypoxia, there is significant PH and RVH. The hypoxia-induced PH in rats is not associated with any disruption of EC, or loss of endothelial Cav1 or Nos3, or enhanced expression of Cav1 in VSMC. Despite the presence of endothelial Cav1 protein, pro-proliferative and anti-apoptotic pathways are activated, indicating Cav1 dysfunction [20, 39]. In addition, the lung sections from infants with respiratory distress syndrome show that the presence of increased pulmonary artery pressure unaccompanied by endothelial damage does not result in the loss of endothelial CAV1 or enhanced expression of *CAV1* in VSMC [19].

In the CM model, the loss of endothelial Cav1 is accompanied by the loss of endothelial proteins such as Pecam1 and soluble guanylate cyclase, and the activation of pro-proliferative and anti-apoptotic pathways leading to PH. At 2 weeks post monocrotaline administration, progressive loss of endothelial Cav1 is associated with PH and RVH in rats [26, 40]. As the disease progresses, a further loss of endothelial Cav1 is accompanied by a loss of von Willebrand factor (vWF), indicative of extensive endothelial damage. Importantly, some of the arteries with vWF loss start to exhibit enhanced expression of CAV1 in VSMC accompanied by increased *Mmp2* expression and activity [40]. At 4 weeks, the significant loss of endothelial Cav1 is accompanied by enhanced expression of *Cav1* in VSMC. The total *Cav1* expression in the lungs increases by 39.14x compared to controls.

Exposing monocrotaline-treated rats to hypoxia (HM group) accelerates the disease process, resulting in significantly higher RVSP and RVH, extensive EC damage and endothelial Cav1 loss accompanied by enhanced expression of Cav1 in VSMC and neointima lesions [26, 40, 41]. Furthermore, 61% of the arteries exhibited enhanced expression of *Cav1* in VSMC; *Cav1* expression in the lungs had increased to 81% of the controls. However, the neointimal lesions in the HM group exhibited loss of Cav1 and normal *Nos3* expression. In the absence of Cav1, Nos3 gets uncoupled and produces nitrosative and oxidative stress. *Cav1* expression is significantly increased (79.06×). It is worthy of note here that the neointimal cells have low *Cav1* and near normal *Nos3* expression, which is a set up for oxidative and nitrosative stress. These results strongly support a dual role of Cav1 in the pathogenesis and the progression of PH, similar to what has been reported in cancer [42, 43].

We found that *Mmp2* was overexpressed by 9.14x in HO, by 39.59x in CM and by 81.47x in HM. MMP2 is known to degrade extracellular matrix and facilitate cell proliferation and migration. Increased *MMP2* expression activity were reported in human PAH [44, 45] and in monocrotaline-induced PH in rats [40].

Many of the upregulated inflammatory genes from Table 1 were also reported by other authors as related to the PH. For instance, *Ccl5* (also known as RANTES; 4.56x in CM and 4,40x in HM), an important chemoattractant for monocytes and T cells, has been shown to be increased in PAH [46]. Interestingly, deletion of *Ccl5* has been shown to attenuate Sugen-hypoxia model of PH via Cav1-dependent amplification of Bmpr2 signaling [47]. As presented in Fig. 2d, we found *Bmpr2* as upregulated by 1.78x in HM, but stayed practically unchanged in HO and CM.

Increased expression of CXCR4, a receptor for the chemokine stromal cell derived factor 1 (SDF1), has been reported in the lungs of patients with IPAH, HPAH and PAH associated with congenital heart defect [48]. Increased Cxcr4 was also reported in Sugen + hypoxia and monocrotalin + hypoxia rodent models of PH [49]. Inhibition of Cxcr4 moderately attenuated pulmonary vascular remodeling in the Sugen + hypoxia model [50] while overexpression of Cxcr4 participates in the repair of tissue injury [51]. In the present study (Table S1), *Cxcr4* was found as up-regulated in CM (4.56x) and HM (2.84x). The lower amplification in HM as compared to CM may be explained by the (even not statistically significant) negative effect of hypoxia (-1.21x in HO). Of note is the up-regulation of the tumor necrosis factors and their receptors, confirming the upstream regulator role of the TNF [1].

Ciapin1 (up-regulated by 3.16x in CM and by 5.16x in HM, Table S1) promotes anti-apoptosis and cell proliferation via the cyclins D1 (Ccnd1) and E1 (Ccne1), and cyclin dependent kinases (Cdk) 2 and 4 [52]. Interestingly, in cell culture, *Ciapin1*siRNA has been shown to inhibit VSMC proliferation and enhance apoptosis by increasing *Bcl2* and *Bax* [53]. Our study confirmed the upregulation for: *Ccnd1* (1.93x in HM), *Cdk4* (1.49x in HO, 4.26x in CM and 5.31x in HM) and *Bax* 2.59x in CM and 2.69x in HM). However, we found *Cdk2* as not regulated and *Ccne1* (-2.78x in HO) and *Bcl2* (-2.47 in HM) as down-regulated.

Among others, we found that *Nfkb1* (nuclear factor kappa B subunit 1), one of the controllers of the cytokine production, was upregulated by 3.50x in CM and by 3.88x in HM (Fig. 1d). *Icam1* (intercellular adhesion molecule 1) was significantly upregulated by 6.79x in HO, 23.65x in CM and 43.97x in HM, while *Vcam1* (vascular cell adhesion molecule 1) was up-regulated by 2.12x in HO, by 6.46x in CM and by 11.25x in HM. *Lgals3* (galectin3), with a critical role in vascular inflammation and fibrosis and heart failure, was also found as up-regulated by 10.89x in CM and 17.83x in HM. Importantly, increased expression of *Lgals3* and *Icam1* has been shown to be present in patients with IPAH and connective tissue disease [54].

Anxa 1 (Annexin A1, increased by 9.64x in HO, 56.48x in CM and 106.00x in HM) plays an essential role in cell invasion, and migration [55]. It is also an anti-inflammatory protein that controls pro-inflammatory mediator release. It promotes leukocyte detachment from EC and serves as a negative regulator of transmigratory processes [56, 57], and provides protection from neointima formation in atherosclerosis [58]. Eng (endoglin, 3.03x in CM and 9.00x in HM), a transmembrane receptor for TGFβ signaling, plays a key role in the balance of Alk1 and Alk5 signaling that regulates EC proliferation. Increased expression of *Alk1*/*Eng* has been reported in EC in IPAH. Furthermore, endoglin deficiency protects mice from hypoxic PH [59]. *Nfat5* (nuclear factor activated T cells 5; 3.59x in HM), is implicated in the regulation of genes associated with migration and proliferation [60, 61]. Our genomic analysis revealed also increased expression of *Edn1*(endothelin 1, 1.88x in HO, 1.83x in CM and 3.11x in HM), *Myc* (myelocytomatosis oncogene, 5.92x in CM and 6.42 in HM), *Pdgfa* (platelet-derived growth factor α, 2.77 in HO, 4.63 in CM and 6.39 in HM).

The complementary effects of the administration of monocrotaline and exposure to hypoxia is perfectly illustrated by the regulation of the six quantified cyclin-dependent kinases, the key regulatory enzymes of the cell-cycle. Thus, *Cdkn2a* was down-regulated in HO and HM groups but not affected in CM, while *Cdkn1a* was down-regulated and *Cdkn1b, Cdkn1c* and *Cdkn2b* were up-regulated in CM and HM groups but not in the HO group. Cyclin-dependent kinases are among the targeted genes for the treatment of pulmonary arterial hypertension [62].

Mitochondria are the major sources of reactive oxygen species (ROS) and highly susceptible to oxidative stress. Increased ROS production and mitochondrial dysfunction occur in a number of diseases including cardiovascular diseases. A significant increase (3.46x) in the expression of *Parp1* (Poly (ADP-ribose) polymerase-1) was found in the lungs of rats exposed to both MCT and hypoxia (HM group). Most of the activity of Parp1 is localized in the nucleus. Recent studies have shown DNA damage and associated increased expression of *Pparp1* to be important aspects of human PAH. Parp1 is implicated in DNA repair, allowing cell proliferation during stress. Parp1 plays an important role in cellular functions during health and disease [63]. Although in humans, PARP1 was reported to up regulate HIF1A, IL6 and NFAT5 [64, 65], we found only *Nfat5* as up-regulated (see above).

Hif1α was down-regulated by -1.72x in HO, by -2.04x in CM and by -1.59x in HM and *Il6* was down-regulated by -3.18x in HM.

Upregulation of other important genes includes: *Slc2a1* (Solute carrier family 2 (facilitated glucose transporter), member 1; 2.94x in HM), *Sod2* (mitochondrial superoxide dismutase; 2.23x in HM), *Hmox1* (hemoxygenase 1; 4.53x in CM and 9.11x in HM), *Gpx1* (glutathione peroxidase 1; 20.48x in HO, 84.91x in CM and 116.90x in HM), *Txn1* (thioredoxin; 7.09x in HO, 54.27x in CM and 93.90x in HM), *Nfe2l2* (Nuclear factor (erythroid-derived-2)-like-2; 3.13x in CM and 5.97 in HM), *Mfn2* (Mitofusin 2; 2.69x in HM), and Nq01 (NAD (P) dehydrogenase quinone 1; 3.50x in CM and 3.97x in HM). *Idh2* (isocitrate dehydrogenase; 4,33x in HO, 16.08x in CM and 28.92x in HM) is an NADPH generating enzyme that plays an important role in regulating mitochondrial redox balance and diminishing stress-induced injury [66]. Low Mfn leads to attenuated angiogenic response to VEGF and eNOS [67].

Recent studies in PAH revealed a metabolic shift towards aerobic glycolysis ("Warburg Effect") similar to what has been observed in cancer, utilized by proliferating cells for survival. Cav1 has been shown to stabilize mitochondria, prevent aerobic glycolysis [25] and negatively regulates NADPH-derived reactive oxygen species [67]. Furthermore, Cav1 modulates Nrf2 expression [68]. It is an important observation that neointimal cells have low Cav1 and normal eNOS expression resulting in oxidative and nitrosative stress [20]. Compared with HO group, in the CM and HM groups, there was significantly increased expression of several antioxidants: *Nfe2l2*, *Prdx2* (Peroxiredoxin 2; 2.66x in HO, 33.94 in CM and 46.01 in HM), *Gpx1*, *Gpx2* (4.92x in HO, 23.70 in CM and 24.47 in HM), *Txn1*, *Sod2*, *Hmox1*, and *Nqo1*. These alterations provide an anti-oxidative and glycolytic milieu for the survival of the proliferating cells.

The analysis of the expression coordination between respiratory and VSMC genes (Fig. 4) revealed several interesting interactions. For instance, in CO, *Rhoa* has no positive partners but has 15 negatives and 1 independent (i.e. 0/15/1) among the 32 ATPases, its coordination power being CP = -74.47%. The situation is reversed in all the three PH models: 9 positives, no negatives, no independents (9/0/0) and a CP of +61.07% in HO, 23/0/1 and a CP of +66.37 in CM and 6/0/3 and a CP of +63.93 in HM. Importantly, 10 of the positively correlated ATPase partners of *Rhoa* in CM were negative partners in CO. This switch from negative to positive correlation of *Rhoa* with the ATPases justifies the reported "role of the Nox4-derived ROS-mediated RhoA/Rho kinase pathway in rat hypertension induced by chronic intermittent hypoxia" [69]. Confirming other reports of increased Rhoa in PH [70], we found *Rhoa* as upregulated by 7.00x in HO, 6.78x in CM and 9.21x in HM. Our results complete the results of a previous report [69] by showing that Rhoa is up-regulated and plays an important role regardless of what caused the PH. Moreover, we found also that *Rhoa*'s action is mediated by the ATPases, a result that needs further investigation.

The Gene Pair Prominence (GPP) analysis demonstrated the plasticity of the genomic fabrics and their interplay. Fig. 5 illustrates how the GPP landscape of the interaction between the vascular smooth muscle contraction (VSMC) genes and the ATPases remodels in the three PH conditions with respect to control. Interestingly, while in control, few VSMC genes interacts with almost all ATPases, in all three PH models almost all VSMC genes interact with few ATPases, making the vascular smooth muscle contraction more vulnerable to certain point alteration within the respiratory chain. This new type of analysis can be used to identify the most important gene pairs in specific interactions.

All PH groups exhibited abnormal expression of genes involved in inflammation and VSMC contractility. Importantly, monocrotaline-treated rat that have been exposed to hypoxia displayed evidence of mitochondrial damage and the activation of antioxidants which are likely to cause metabolic switch and provide a survival milieu for the proliferating cells.

Supplementary Materials: The following are available online at www.mdpi.com/xxx/s1, Table S1: Regulation of important genes involved in the immune-inflammatory response, Table S2: Regulation of mitochondrial genes.

Author Contributions: conceptualization: R.M, and D.A.I.; methodology: R.M., S.I. and D.A.I.; software: D.A.I.; validation: R.M. and S.I.; formal analysis: S.I. and D.A.I.; investigation: J.H. and S.I.; resources, R.M. and D.A.I.; data curation, D.A.I., and R.M.; writing: D.A.I. and R.M.; visualization, D.A.I. and R.M.; supervision, R.M. and D.A.I.; project administration, R.M. and D.A.I.; funding acquisition, R.M. and D.A.I.

Funding: R.M., J.H. and S.I. were supported by an NYMC intramural grant. D.A.I. was supported by the Chancellor's Research Initiative (CRI) funding for the Center for Computational Systems Biology at the Prairie View A&M University.

Conflicts of Interest: The authors declare no conflict of interest

Appendix A

Table S1

Gene	Description	HO/CO	CUT	CM/CO	CUT	HM/CO	CUT
Ccl11	chemokine (C-C motif) ligand 11	1.19	1.95	1.36	1.95	3.56	1.72
Ccl17	chemokine (C-C motif) ligand 17	-1.10	1.76	2.21	1.76	1.49	1.39
Ccl19	chemokine (C-C motif) ligand 19	2.84	2.59	7.88	2.59	17.82	2.72
Ccl2	chemokine (C-C motif) ligand 2	2.18	2.18	3.58	2.18	5.12	1.74
Ccl3	chemokine (C-C motif) ligand 3	1.41	1.13	2.29	1.13	2.76	1.45
Ccl7	chemokine (C-C motif) ligand 7	-1.01	1.39	1.52	1.39	1.95	1.74
Ciapin1	cytokine induced apoptosis inhibitor 1	1.40	2.08	3.16	2.08	5.16	1.35
Crlf1	cytokine receptor-like factor 1	4.15	3.32	10.68	3.32	12.63	1.53
Crlf2	cytokine receptor-like factor 2	1.38	3.04	2.91	3.04	4.13	1.99
Crlf3	cytokine receptor-like factor 3	1.30	1.25	2.09	1.25	2.54	1.55
Cxcl1	chemokine (C-X-C motif) ligand 1 (melanoma growth stimulating activity, alpha)	1.52	1.20	4.48	1.20	5.56	1.71
Cxcl14	chemokine (C-X-C motif) ligand 14	6.99	2.67	15.02	2.67	15.57	1.69
Cxcl16	chemokine (C-X-C motif) ligand 16	2.21	2.57	11.83	2.57	15.54	1.28
Cxcl17	chemokine (C-X-C motif) ligand 17	9.78	2.87	26.72	2.87	27.68	1.55
Cxcl2	chemokine (C-X-C motif) ligand 2	1.00	1.22	1.96	1.22	1.10	2.03
Cxcr1	chemokine (C-X-C motif) receptor 1	1.24	1.26	1.93	1.26	2.25	1.66
Cxcr4	chemokine (C-X-C motif) receptor 4	-1.21	2.38	4.56	2.38	2.84	1.78
Cxcr7	chemokine (C-X-C motif) receptor 7	-1.02	1.12	1.35	1.12	2.33	1.64
Cytl1	cytokine like 1 (Cytl1)	1.14	1.25	1.26	1.25	-1.56	1.75
Ifi27	interferon, alpha-inducible protein 27	35.46	2.77	57.06	3.05	57.04	2.09
Ifi27l2b	interferon, alpha-inducible protein 27 like 2B	8.92	2.60	39.94	3.32	62.37	2.19
Ifi30	interferon gamma inducible protein 30	4.83	3.19	42.25	2.53	49.68	1.33
Ifi35	interferon-induced protein 35	-1.08	1.55	1.94	1.96	2.65	1.94
Ifi47	interferon gamma inducible protein 47	1.05	1.09	1.50	1.95	1.29	1.25
Ifit2	interferon-induced protein with tetratricopeptide repeats 2	1.13	1.41	1.76	2.07	2.32	1.55
Ifit3	interferon-induced protein with tetratricopeptide repeats 3	1.01	1.37	2.29	2.40	2.25	1.78
Ifitm1	interferon induced transmembrane protein 1	1.28	2.22	10.29	3.08	20.26	1.81
Ifitm2	interferon induced transmembrane protein 2	-1.15	3.14	19.39	3.15	36.04	2.22
Ifitm3	interferon induced transmembrane protein 3	-1.16	2.47	9.57	2.75	19.11	1.81
Ifngr1	interferon gamma receptor 1	1.50	3.28	17.75	2.54	16.54	1.85
Ifrd1	interferon-related developmental regulator 1	1.08	1.37	2.90	1.97	3.26	1.80
Ifrd2	interferon-related developmental regulator 2	1.29	1.45	1.92	1.75	2.24	1.41
Ik	IK cytokine	1.73	2.11	3.60	2.11	4.52	1.36
Il10rb	interleukin 10 receptor, beta	-1.08	2.94	2.28	2.94	3.88	1.84
Il12b	interleukin 12B	1.54	1.47	-1.06	1.47	-1.94	2.40
Il16	interleukin 16	1.38	1.92	3.07	1.92	5.52	1.32
Il17ra	interleukin 17 receptor A	3.00	2.65	7.66	2.65	14.06	1.40
Il17re	interleukin 17 receptor E	1.33	2.50	2.71	2.50	4.34	1.25
Il18	interleukin 18	1.39	1.37	5.78	1.37	5.86	1.53
Il1a	interleukin 1 alpha	1.01	1.61	1.83	1.61	1.50	1.62
Il1r2	interleukin 1 receptor, type II	1.49	1.09	4.70	1.09	2.44	1.74
Il1rn	interleukin 1 receptor antagonist	-1.30	1.85	1.89	1.85	2.55	1.74
Il34	interleukin 34	5.71	3.33	18.05	3.33	27.98	1.40
Il6st	interleukin 6 signal transducer	2.75	2.16	7.87	2.16	13.02	1.46
Ilf3	interleukin enhancer binding factor 3	-1.17	1.55	1.26	1.55	1.51	1.50
Tnfaip8	tumor necrosis factor, alpha-induced protein 8	3.70	2.74	5.19	2.23	6.99	1.40
Tnfaip8l2	tumor necrosis factor, alpha-induced protein 8-like 2	4.39	2.62	8.29	2.64	20.10	1.60
Tnfrsf11a	tumor necrosis factor receptor superfamily, member 11a, NFKB activator	1.83	1.73	-1.51	2.12	-1.98	1.73
Tnfrsf12a	tumor necrosis factor receptor superfamily, member 12a	-1.64	1.67	3.16	2.80	3.98	1.67
Tnfrsf14	tumor necrosis factor receptor superfamily, member 14	1.04	1.20	1.48	1.43	1.38	1.47
Tnfrsf1a	tumor necrosis factor receptor superfamily, member 1a	5.32	2.70	6.12	2.71	12.67	1.45
Tnfrsf21	tumor necrosis factor receptor superfamily, member 21	1.57	1.74	3.96	2.49	2.17	1.46
Tnfrsf26	tumor necrosis factor receptor superfamily, member 26	1.56	1.72	1.97	1.75	2.82	1.52
Tnfsf13	tumor necrosis factor (ligand) superfamily, member 13	1.13	2.32	6.87	2.43	5.98	1.64

Table S1: Regulation of important genes involved in the immune-inflammatory response. Significant (larger than CUT) absolute fold-changes are in red background for up-regulated and green background for down-regulated. Note the range of the CUTs, from 1.12 (for the regulation of *Cxcr7* in CM vs CO) to 3.33 (for the regulation of *Il34* in both HO and CM vs. CO). Our procedure to determine the cut-off for the absolute fold-change for every gene in each comparison instead of using a fixed cut-off (like 1.5x) identified additional regulated genes (CUT in yellow background, e.g. *Ccl7*

591 in HO/CO). It also eliminated the false regulations (expression ratio in grey background, e.g. *Cxcl16*
592 in HO/CO) whose absolute (although over 1.5x fold-change) was below the CUT (2.57) computed for
593 that gene in the compared conditions.

594

Gene	Description	HO/CO	CUT	CM/CO	CUT	HM/CO	CUT
Mrpl10	mitochondrial ribosomal protein L10	18.83	3.01	13.96	1.53	16.23	2.54
Mrpl13	mitochondrial ribosomal protein L13	2.18	2.58	7.52	2.58	13.92	1.76
Mrpl14	mitochondrial ribosomal protein L14	2.41	3.29	1.57	3.01	2.32	2.88
Mrpl17	mitochondrial ribosomal protein L17	3.56	3.04	14.88	2.76	25.82	1.66
Mrpl19	mitochondrial ribosomal protein L19	1.82	1.82	1.17	1.96	1.76	1.59
Mrpl2	mitochondrial ribosomal protein L2	-1.70	2.77	-1.02	2.64	1.40	2.11
Mrpl20	mitochondrial ribosomal protein L20	-1.25	3.28	2.07	3.15	3.22	2.30
Mrpl23	mitochondrial ribosomal protein L23	-3.37	2.99	-1.96	2.95	-1.42	2.24
mrpl24	mitochondrial ribosomal protein L24	-1.00	2.29	1.87	2.60	2.90	2.07
Mrpl27	mitochondrial ribosomal protein L27	2.27	3.16	4.80	2.82	6.80	1.92
Mrpl28	mitochondrial ribosomal protein L28	3.22	3.48	4.11	3.07	6.62	2.46
Mrpl34	mitochondrial ribosomal protein L34	-2.41	3.24	1.28	2.96	2.20	2.17
Mrpl35	mitochondrial ribosomal protein L35	3.08	2.13	2.09	1.87	2.05	1.70
Mrpl37	mitochondrial ribosomal protein L37	-1.65	3.10	1.16	2.92	1.98	2.15
Mrpl38	mitochondrial ribosomal protein L38	-4.33	2.46	-3.15	2.50	-2.70	2.10
Mrpl40	mitochondrial ribosomal protein L40	-2.54	2.05	-2.31	2.06	-1.66	1.87
Mrpl41	mitochondrial ribosomal protein L41	1.79	2.49	6.10	2.59	10.69	1.69
Mrpl42	mitochondrial ribosomal protein L42	-3.32	2.02	-1.96	2.32	-1.44	2.00
Mrpl45	mitochondrial ribosomal protein L45	2.39	2.61	5.24	2.66	8.00	1.61
Mrpl48	mitochondrial ribosomal protein L48	-6.50	3.23	-3.66	2.90	-2.21	2.48
Mrpl54	mitochondrial ribosomal protein L54	-1.10	3.32	3.80	3.16	5.78	2.29
Mrpl9	mitochondrial ribosomal protein L9	3.14	2.93	6.66	2.61	13.75	1.81
Mrps12	mitochondrial ribosomal protein S12	2.13	2.86	4.22	2.66	5.81	1.80
Mrps15	mitochondrial ribosomal protein S15	1.24	1.91	1.59	1.68	1.57	1.77
Mrps2	mitochondrial ribosomal protein S2	-4.43	2.19	-3.83	2.27	-5.21	2.17
Mrps21	mitochondrial ribosomal protein S21	-2.74	2.18	-2.45	2.15	-3.18	2.28

619 **Table S2: Regulation of mitochondrial genes.** Significant (larger than CUT) absolute fold-changes
620 are in red background for up-regulated and green background for down-regulated. Note the range
621 of the CUTs, from 1.53 (for the regulation of Mrpl10 in CM vs CO) to 3.48 (for the regulation of *Mrpl28*
622 in HO vs. CO). Our procedure to determine the cut-off for the absolute fold-change for every gene in
623 each comparison instead of using a fixed cut-off (like 1.5x) eliminated the false regulations
624 (expression ratio in grey background, e.g. *Mrpl13* in HO/CO) whose absolute (although over 1.5x
625 fold-change) was below the CUT (2.58) computed for that gene in the compared conditions.

626

References

1. Stearman, R.S.; Bui, Q.M.; Speyer, G.; Handen, A.; Cornelius, A.R.; Graham, B.B. et al. Systems Analysis of the Human Pulmonary Arterial Hypertension Lung Transcriptome. *Am J Respir Cell Mol Biol* **2019**, 60(6):637-649. doi: 10.1165/rcmb.2018-0368OC.
2. Simonneau, G.; Gatzoulis, M.A.; Adatia, I.; Celemajer, D.; Denton, C. et al. Updated clinical classification of pulmonary hypertension. *J Am Coll Cardiol* **2014**, 62 (25, suppl): D34-D41.
3. D'Alonzo, G.C.; Barst, R.J.; Ayers, S.M.; Bergofsky, E.H.; Brundage, B.H. et al. Survival in patients with primary pulmonary hypertension: results from a national registry. *Ann Intern Med* **1991**, 115:343-349. DOI: 10.7326/0003-4819-115-5-343
4. Pogoriler, J.E.; Rich, S.; Archer, S.L.; Husain, A.N. Persistence of complex vascular lesions despite prolonged prostacyclin therapy of pulmonary arterial hypertension. *Histopathology* **2012**, 61:597- 609. DOI: 10.1111/j.1365-2559.2012.04246.x
5. Sakao, S.; Tatsumi, K.; Voelkel, N.F. Reversible or irreversible remodeling in pulmonary arterial hypertension. *Am J Respir Cell Mol Biol* **2010**, 43:629-634. DOI: 10.1165/rcmb.2009-0389TR.
6. Humbert, M.; Sitbon, O.; Yaïci, A.; Montani, D.; O'Callaghan, D.S. et al. Survival in incident and prevalent cohorts of patients with pulmonary arterial hypertension. *Eur Respir J* **2010**, 36:549-555. doi: 10.1183/09031936.00057010
7. Farber, H.W.; Miller, D.P.; Poms, A.D.; Badesch, D.B.; Frost, A.E.; Muros-Le Rouzic, E. et al. Five-Year outcomes of patients enrolled in the REVEAL Registry. *Chest* **2015**, 148:1043-1054. DOI: 10.1378/chest.15-0300.
8. Murakami, K.; Mathew, R.; Huang, J.; Farahami, R.; Peng, H.; Olson, S.C. et al. Smurf1 ubiquitin ligase causes downregulation of BMP receptors and is induced in monocrotaline and hypoxia models of pulmonary arterial hypertension. *Expt Biol Med* **2010**, 235:805-813. DOI: 10.1258/ebm.2010.009383
9. McMurtry, M.S.; Moudgil, R.; Hashimoto, K.; Bonnet, S.; Michelakis, E.D.; Archer, S.L. Overexpression of human bone morphogenetic protein receptor 2 does not ameliorate monocrotaline pulmonary arterial hypertension. *Am J Physiol Lung Cell Mol Phsyiol* **2007**, 292:L872-L878. DOI: 10.1152/ajplung.00309.2006
10. Long, L.; Ormiston, M.L.; Yang, X.; Southwood, M.; Gräf, S.; Machado, R.D. et al. Selective enhancement of endothelial BMPR-II with BMP9 reverses pulmonary arterial hypertension. *Nat Med* **2015**, 21:777-785. DOI: 10.1038/nm.3877
11. Mathew, R. Pulmonary Hypertension: Endothelial cell Function. In *Pulmonary hypertension: From Bench Research to Clinical Challenge*; Sulica, R., Preston, I. Eds; IntechOpen, London, UK, **2011**, pp 1-24. ISBN 978-953-307-835-9 (DOI:10.5772/26198).
12. Li, M.; Vattulainen, S.; Aho, J.; Orcholski, M.; Rojas, V.; Yuan, K. et al. Loss of bone morphogenetic protein receptor 2 is associated with abnormal DNA repair in pulmonary arterial hypertension. *Am J Respir C Mol Biol* **2014**, 50:1118-1128. DOI: 10.1165/rcmb.2013-0349OC
13. Rothman, A.M.; Arnold, N.D.; Pickworth, J.A.; Iremonger, J.; Ciuclan, L.; Allen, R.M. et al. MicroRNA-140-5p and SMURF1 regulate pulmonary arterial hypertension. *J Clin Invest* **2016**, 126:2495-2508. DOI: 10.1172/JCI83361
14. Mason, N.A.; Springall, D.R.; Burke, M.; Pollock, J.; Mikhail, G.; Yacoub, M.H. et al. High expression of endothelial nitric oxide synthase in plexiform lesions of pulmonary hypertension. *J Path* **1998**, 185:313-318. DOI: 10.1002/(SICI)1096-9896(199807)185:3<313::AID-PATH93>3.0.CO;2-8
15. Austin, E.D.; Ma, L.; LeDuc, C.; Berman-Rozenzweig, E.; Borczuk, A.; Phillips, J.A. et al. Whole exon sequence to identify a novel gene (caveolin-1) associated with human pulmonary arterial hypertension. *Circ Cardiovasc Genet* **2012**, 5:336-343. doi: 10.1161/CIRCGENETICS.111.961888.
16. Zhao, Y.Y.; Liu, Y.; Stan, R.V.; Fan, L.; Gu, Y.; Dalton, N. et al. Defects in caveolin-1 cause dilated cardiomyopathy and pulmonary hypertension in knockout mice. *Proc Natl Acad Sci* **2002**, 99:11375-11
17. Murata, T.; Lin, M.I.; Huang, Y.; Yu, J.; Bauer, P.M.; Giordano, F.G. et al. Reexpression of caveolin-1 in endothelium rescues the vascular, cardiac, and pulmonary defects in global caveolin-1 knockout mice. *J Exp Med* **2007**, 204:2373-2382. DOI: 10.1084/jem.20062340
18. Patel, H.H.; Zhang, S.; Murray, F.; Suda, R.Y.; Head, B.P.; Yokoyama, U. et al.. Increased smooth muscle cell expression of caveolin-1 and caveolae contribute to the pathophysiology of idiopathic pulmonary arterial hypertension. *FASEB J* **2007**, 21:2970-2979. DOI: 10.1096/fj.07-8424com

19. Dereddy, N.; Hunag, J.; Erb, M.; Guzel, S.; Wolk, J.H.; Sett, S.S. et al. Associated inflammation or increased flow-mediated shear stress, but not the pressure alone disrupts endothelial caveolin-1 in infants with pulmonary hypertension. *Pulm Circ* **2012**, 2:492-500. doi: 10.4103/2045-8932.105038
20. Huang, J.; Wolk, J.H.; Gewitz, M.H.; Loyd, J.E.; West, J.; Austin, E.D. et al. Enhanced caveolin-1 expression in smooth muscle cells: Possible prelude to neointima formation. *World J Cardiol* **2015**, 7:671-684. DOI: 10.4330/wjc.v7.i10.671
21. Codrici, E.; Albulescu, L.; Popescu, I.D.; Mihai, S.; Enciu, A.M.; Albulescu, R. et al. Caveolin-1-Knockout Mouse as a Model of Inflammatory Diseases. *J Immunol Res* **2018,** 2498576. doi: 10.1155/2018/2498576.
22. Jasmin, J.F.; Mercier, I.; Dupuis, J.; Tanowitz, H.B.; Lisanti, M.P. Short-term administration of a cell-permeable caveolin-1 peptide prevents the development of monocrotaline-induced pulmonary hypertension and right ventricular hypertrophy. *Circulation* **2006**, 114:912-920. DOI: 10.1161/CIRCULATIONAHA.106.634709.
23. Huang, J.; Kaminski, P.M.; Edwards, J.G.; Yeh, A.; Wolin, M.S.; Frishman, W.H. et al. Pyrrolidine dithiocarbamate restores endothelial cell membrane integrity and attenuates monocrotaline-induced pulmonary artery hypertension. *Am J Physiol Lung Cell Mol Physiol* **2008**, 294: L1250-L1259. DOI: 10.1152/ajplung.00069.2007
24. Bakhshi, F.R.; Mao, M.; Shajahan, A.N.; Piegeler, T.; Chen, Z.; Chernaya, O. et al. Nitrosation-dependent caveolin 1 phosphorylation, ubiquitination, and degradation and its association with idiopathic pulmonary arterial hypertension. *Pulm Circ* **2013,** 3:816-830. doi: 10.1086/674753.
25. Shiroto, T.; Romero, N.; Sugiyama, T.; Sartoretto, J.L.; Kalwa, H.; Yan, Z. et al. Caveolin-1 is a critical determinant of autophagy, metabolic switching, and oxidative stress in vascular endothelium. *PLoS One* **2014,** 9:e87871. DOI: 10.1371/journal.pone.0087871
26. Huang, J.; Wolk, J.; Gewitz, M.H.; Mathew, R. Progressive Endothelial Cell Damage in an Inflammatory Model of Pulmonary Hypertension. *Expt Lung Res* **2010**, 36:57-66. DOI: 10.3109/01902140903104793
27. Kravchick DO, Hrdinka M, Iacobas S, Iacobas DA, Kreutz MR and Jordan BA. Synaptonuclear messenger PRR7 inhibits c-Jun ubiquitination and regulates NMDA mediated excitotoxicity. *EMBOJ* **2016**, 35(17):1923-34. doi: 10.15252/embj.201593070.
28. Fan, C.; Iacobas, D.A.; Zhou, D.; Chen, Q.; Lai, J.K.; Gavrialov, O.; Haddad, G.G. Gene expression and phenotypic characterization of mouse heart after chronic constant or intermittent hypoxia. *Physiol Genomics* **2005**, 22:292-307. DOI: 10.1152/physiolgenomics.00217.2004
29. Iacobas, D.A.; Iacobas, S.; Nebieridze, N.; Velisek, L.; Veliskova, J. Estrogen protects neurotransmission transcriptome during status epilepticus, *Front Neurosci* **2018**, 12:332. DOI: 10.3389/fnins.2018.00332.
30. Iacobas, S.; Ede, N.; Iacobas, D.A. The Gene Master Regulators (GMR) Approach Provides Legitimate Targets for Personalized, Time-Sensitive Cancer Gene Therapy. *Genes* **2019**, 10(8), 560. doi:10.3390/genes10080560.
31. Iacobas, D.A.; Iacobas, S.; Tanowitz, H.B.; deCarvalho, A.C.; Spray, D.C. Functional genomic fabrics are remodeled in a mouse model of Chagasic cardiomyopathy and restored following cell therapy. *Microbes Infect* **2018**, 20(3), 185-195. doi: 10.1016/j.micinf.2017.11.003.
32. Kanehisa, M.; Furumichi, M.; Tanabe, M.; Sato, Y.; Morishima, K. KEGG: new perspectives on genomes, pathways, diseases and drugs. *Nucleic Acids Res* **2017**, 45, D353-D361 (2017). DOI: 10.1093/nar/gkw1092
33. Iacobas, D.A.; Chachua, T.; Iacobas, S.; Benson, M.J.; Borges, K.; Veliskova, J.; Velisek, L. ACTH and PMX53 recover the normal synaptic transcriptome in a rat model of infantile spasms. *Sci Rep* **2018**, 8(1):5722. DOI:10.1038/s41598-018-24013-x
34. Iacobas, D.A.; Fan, C.; Iacobas, S.; Spray, D.C.; Haddad, G.G. Transcriptomic changes in developing kidney exposed to chronic hypoxia. *Biochem Biophys Res Comm* **2006**, 349(1), 329-338. DOI:10.1016/j.bbrc.2006.08.056.
35. Iacobas, D.A.; Fan, C.; Iacobas, S.; Haddad, G.G. Integrated transcriptomic responses to cardiac chronic hypoxia: translational regulators and response to stress in cell survival. *Func Integr Genomics* **2008**, 8(3):265-275. PMCID:PMC2856931
36. Iacobas, D.A.; Iacobas, S.; Haddad, G.G. Heart rhythm genomic fabric in hypoxia. *Biochem Biophys Res Commun* **2010**. 391(4):1769-1774. doi: 10.1016/j.bbrc.2009.12.151
37. Iacobas, D.A.; Iacobas, S.; Spray, D.C. Connexin43 and the brain transcriptome of the newborn mice. *Genomics* **2007**, 89(1), 113-123. DOI:10.1016/j.ygeno.2006.09.007.

38. Iacobas, D.A.; Iacobas, S.; Lee, P.R.; Cohen, J.E. Fields, R.D. Coordinated Activity of Transcriptional Networks Responding to the Pattern of Action Potential Firing in Neurons. *Genes* **2019**, 10(10), 754; doi.org/10.3390/genes10100754.
39. Huang, J.; Frid, M.; Gewitz, M.H.; Fallon, J.T.; Brown, D.; Krafuser, G. et al. Hypoxia-induced Pulmonary Hypertension and Chronic Lung Disease: Caveolin-1 Dysfunction an Important Underlying Feature. *Pulm Circulation* **2019**, 9(1):2045894019837876. doi: 10.1177/2045894019837876.
40. Huang, J.; Wolk, J.H.; Gewitz, M.H.; Mathew, R. Caveolin-1 expression during the progression of pulmonary hypertension. *Exp Biol Med* **2012**, 237:956-965. DOI: 10.1258/ebm.2012.011382
41. Mathew, R.; Huang, J.; Shah, M.; Patel, K.; Gewitz, M.; Sehgal, P.B. Disruption of endothelial-cell caveolin-1 alpha/raft scaffolding during development of monocrotaline-induced pulmonary hypertension. *Circulation* **2004**, 110:1499-506. DOI: 10.1161/01.CIR.0000141576.39579.23
42. Mathew, R. Cell-specific dual role of caveolin-1 in pulmonary hypertension. *Pulm Med* **2011**, 2011: 573432. DOI: 10.1155/2011/573432
43. Mathew, R. Pathogenesis of pulmonary hypertension: a case for caveolin-1 and cell membrane integrity. *Am J Physiol Heart Circ Physiol* **2014**, 306:H15-H25. DOI: 10.1152/ajpheart.00266.2013
44. Lepetit, H.; Eddahibi, S.; Fadel, E.; Frisdal, E.; Munaut, C.; Noel, A. *et al*. Smooth muscle cell matrix metalloproteinases in idiopathic pulmonary arterial hypertension. *Eur Respir J* **2005**, 25:834-842. DOI: 10.1183/09031936.05.00072504
45. Tiede, S.L.; Wassenberg, M.; Christ, K.; Schermuly, R.T.; Seeger, W.; Grimminger, F. *et al*. Biomarkers of tissue remodeling predict survival in patients with pulmonary hypertension. *Int J Cardiol* **2016**, 223:821-826. DOI: 10.1016/j.ijcard.2016.08.240
46. Dorfmüller, P.; Zarka, V.; Durand-Gasselin, I.; Monti, G.; Balabanian, K.; Garcia, G. *et al*. Chemokine RANTES in severe pulmonary arterial hypertension. *Am J Respir Crit Care Med* **2002**, 165:534-539. DOI: 10.1164/ajrccm.165.4.2012112
47. Nie, X.; Tan, J.; Dai, Y.; Liu, Y.; Zou, J.; Sun, J.; *et al*. CCL5 deficiency rescues pulmonary vascular dysfunction, and reverses pulmonary hypertension via caveolin-1-dependent BMPR2 activation. *J Mol Cell Cardiol* **2018**, 116:41-56. DOI: 10.1016/j.yjmcc.2018.01.016
48. Toshner, M.; Voswinckel, R.; Southwood, M.; Al-Lamki, R.; Howard, L.S.; Marchesan, D. *et al*. Evidence of dysfunction of endothelial progenitors in pulmonary arterial hypertension. *Am J Respir Crit Care Med* **2009**, 180:780-787. doi: 10.1164/rccm.200810-1662OC
49. Zhang, T.; Kawaguchi, N.; Hayama, E.; Furutani, Y.; Nakanishi, T. High expression of CXCR4 and stem cell markers in a monocrotaline and chronic hypoxia-induced rat model of pulmonary arterial hypertension. *Exp Therap Med* **2018**, 15:4615-4622. doi: 10.3892/etm.2018.6027
50. Farkas, D.; Kraskauskas, D.; Drake, J.I.; Alhussaini, A.A.; Kraskauskiene, V.; Bogaard, H.J.; *et al*. CXCR4 inhibition ameliorates severe obliterative pulmonary hypertension and accumulation of C-kit$^+$cells in rats. *PLoS One* **2014**, 9(2):e89810. DOI: 10.1371/journal.pone.0089810
51. Yang, J.X.; Zhang, N.; Wang, H.W.; Gao, P.; Yang, Q.P.; Wen, Q.P. CXCR4 receptor overexpression in mesenchymal stem cells facilitates treatment of acute lung injury in rats. *J Biol Chem* **2015** 290:1994-2006. doi: 10.1074/jbc.M114.605063
52. Huang, Z.; Su, G.F.; Hu, W.J.; Bi, X.X.; Zhang, L; Wan, G. The study on expression of CIAPIN1 interfering hepatocellular carcinoma cell proliferation and its mechanisms. *Eur Rev Med Pharmacol Sci* **2017**, 21(13):3054-3060.
53. Yang, Z.; Wang, W.E.; Zhang, Q. CIAPIN1 siRNA inhibits proliferation, migration and promotes apoptosis of VSMCs by regulating Bcl-2 and Bax. *Curr Neurovasc Res* **2013**, 10(1):4-10.
54. Clavier, L.; Legchenko, E.; Grimm, L.; Sallmon, H.; Hatch, A.; Plouff, B.D. *et al*. Galectin 3 and aldosterone as potential tandem biomarkers in pulmonary arterial hypertension. *Heart* **2016**, 102:390-396. doi: 10.1136/heartjnl-2015-308365.
55. Perretti, M.; Ingegnoli, F.; Wheller, S.K.; Blades, M.C.; Solito, E.; Pitzalis, C. Annexin 1 modulates monocyte-endothelial cell interaction in vitro and cell migration in vivo in the human SCID mouse transplantation model. *J Immunol* **2002**, 169:2085-2092. DOI: 10.4049/jimmunol.169.4.2085
56. Drechsler, M.; de Jong, R.; Rossaint, J.; Viola, J.R.; Leoni, G.; Wang, J.M. *et al*. Annexin A1 counteracts chemokine-induced arterial myeloid cell recruitment. *Circ Res* **2005**, 116: 827-835. DOI: 10.1161/CIRCRESAHA.116.305825

57. Sheikh, M.H.; Solito, E. Annexin A1: Uncovering the Many Talents of an Old Protein. *Int J Mol Sci* **2018**, 19(4). pii: E1045. doi: 10.3390/ijms19041045.
58. de Jong, R.J.; Paulin, N.; Lemnitzer, P.; Viola, J.R.; Winter, C.; Ferraro, B. *et al*. Protective Aptitude of Annexin A1 in Arterial Neointima Formation in Atherosclerosis-Prone Mice-Brief Report. *Arterioscler Thromb Vasc Biol* **2017**, 37:312-315. doi: 10.1161/ATVBAHA.116.308744
59. Gore, B.; Izikki, M.; Mercier, O.; Dewachter, L.; Fadel, E.; Humbert, M. *et al.* Key role of the endothelial TGF-β/ALK1/endoglin signaling pathway in humans and rodents pulmonary hypertension. *PloS One* **2014**, 9(6): e100310. doi: 10.1371/journal.pone.0100310. eCollection 2014.
60. Scherer, C.; Pfisterer, L.; Wagner, A.H.; Hödebeck, M.; Cattaruzza, M.; Hecker, M. *et al*. Arterial wall stress controls NFAT5 activity in vascular smooth muscle cells. *J Am Heart Assoc* **2014**, 10;3(2): e000626. DOI: 10.1161/JAHA.113.000626
61. Cao, W.; Zhang, D.; Li, Q.; Liu, Y.; Jing, S.; Cui, J. *et al*. Biomechanical Stretch Induces Inflammation, Proliferation, and Migration by Activating NFAT5 in Arterial Smooth Muscle Cells. *Inflammation* **2017**, 40:2129-2136. doi: 10.1007/s10753-017-0653-y.
62. Weiss, A.; Neubauer, M.C.; Yerabolu, D.; Kojonazarov, B.; Schlueter, B.C.; Neubert, L. *et al*. Targeting cyclin-dependent kinases for the treatment of pulmonary arterial hypertension. *Nat Commun* **2019**, 10(1):2204. doi: 10.1038/s41467-019-10135-x.
63. Brunyanszki, A.; Szczesny, B.; Virág, L.; Szabo, C. Mitochondrial poly(ADP-ribose) polymerase: The Wizard of Oz at work. *Free Radic Biol Med* **2016**, pii: S0891-5849(16)00075-7. doi: 10.1016/j.freeradbiomed.2016.02.024.
64. Elser, M.; Borsig, L.; Hassa, P.O.; Erener, S.; Messner, S.; Valovka, T. *et al*. Poly(ADP-ribose) polymerase 1 promotes tumor cell survival by coactivating hypoxia-inducible factor-1-dependent gene expression. *Mol Cancer Res* **2008**, 6:282-290. DOI: 10.1158/1541-7786.MCR-07-0377
65. Meloche, J.; Pflieger, A.; Vaillancourt, M.; Paulin, R.; Potus, F.; Zervopoulos, S. *et al*. Role for DNA damage signaling in pulmonary arterial hypertension. *Circulation* **2014**, 129:786-797. DOI: 10.1161/CIRCULATIONAHA.113.006167
66. Park, J.B.; Nagar, H.; Choi, S.; Jung, S.B.; Kim, H.W.; Kang, S.K. *et al*. IDH2 deficiency impairs mitochondrial function in endothelial cells and endothelium-dependent vasomotor function. *Free Rad Biol Med* **2016**, 94:36-46. DOI: 10.1016/j.freeradbiomed.2016.02.017
67. Lugus, J.J. Ngoh, G.A.; Bachschmid, M.M.; Kenneth, K. Mitofusins are required for angiogenic function and modulate different signaling pathways in cultured endothelial cells. *J Mol Cell Cardiol* **2011**, 51:885-893. doi: 10.1016/j.yjmcc.2011.07.023
68. Chen, F.; Barman, S.; Yu, Y.; Haigh, S.; Wang, Y.; Black, S.M. et al. Caveolin-1 is a negative regulator of NADPH oxidase-derived reactive oxygen species. *Free Rad Biol Med* **2014**, 73:201-213. doi: 10.1016/j.freeradbiomed.2014.04.029
69. Hart, P.C., Ratti, B.A.; Mao, M.; Ansenberger-Fricano, K.; Shajahan-Haq, A.N.; Tyner, A.L. *et al*. -1 regulates cancer cell metabolism via scavenging Nrf2 and suppressing MnSOD-driven glycolysis. *Oncotarget* **2016**, 7:308-322. DOI: 10.18632/oncotarget.5687
70. Lu, W.; Kang, J.; Hu, K.; Tang, S.; Zhou, X.; XU, L. *et al*. The role of the Nox4-derived ROS-mediated RhoA/Rho kinase pathway in rat hypertension induced by chronic intermittent hypoxia. *Sleep Breath* **2017**, 21(3):667-677. doi: 10.1007/s11325-016-1449-2
71. Oka, M.; Fagan, K.A.; Jones, P.L.; McMurtry, I.F. Therapeutic potential of RhoA/Rho kinase inhibitors in pulmonary hypertension. *Br J Pharmacol* **2008**, 155:444-454. DOI: 10.1038/bjp.2008.239